

RR Lyrae stars in four globular clusters in the Fornax dwarf galaxy

A. D. Mackey^{1*} and G. F. Gilmore¹

¹*Institute of Astronomy, University of Cambridge, Madingley Road, Cambridge CB3 0HA*

Accepted –. Received –

ABSTRACT

We have surveyed four of the globular clusters in the Fornax dwarf galaxy (clusters 1, 2, 3, and 5) for RR Lyrae stars, using archival F555W and F814W *Hubble Space Telescope* observations. We identify 197 new RR Lyrae stars in these four clusters, and 13 additional candidate horizontal branch variable stars. Although somewhat restricted by our short observational baseline, we derive periods and light-curves for all of the stars in the sample, and calculate photometric parameters such as mean magnitudes and colours. This is the first time that RR Lyrae stars in the Fornax globular clusters have been quantitatively identified and measured. We find that the Fornax clusters have exceptionally large specific frequencies of RR Lyrae stars, in comparison with the galactic globular clusters. It is likely that Fornax 1 has the largest specific frequency measured in *any* globular cluster. In addition, the Fornax clusters are unusual in that their RR Lyrae populations possess mean characteristics intermediate between the two Oosterhoff groups defined by the galactic globular clusters. In this respect the RR Lyrae populations in the Fornax clusters most closely resemble the *field* populations in several dwarf galaxies. Fornax 5 has an unusually large fraction of RRc stars, and also possesses several strong RRe (second overtone pulsator) candidates.

With a large sample of horizontal branch variable stars available to us, we revise previous measurements of the horizontal branch morphology in each cluster. The Fornax clusters most closely resemble the “young” galactic halo population defined by Zinn in that their horizontal branch morphologies are systematically redder than many galactic clusters of similar metallicity. We also confirm the existence of the second parameter effect among the Fornax clusters, most markedly between clusters 1 and 3. The edges of the instability strip are well defined in several of the Fornax clusters, and we are able to make measurements of the intrinsic $V - I$ colours of these edges. Finally, we determine foreground reddening and distance estimates for each cluster. We find a mean distance modulus to the Fornax dwarf of $(m - M)_0 = 20.66 \pm 0.03$ (random) ± 0.15 (systematic). Our measurements are consistent with a line of sight depth of $\sim 8 - 10$ kpc for this galaxy, which is in accordance with its dimensions as measured in the plane of the sky. This approximately spherical shape for Fornax is incompatible with tidal model explanations for the observed high internal stellar velocity dispersions in many dwarf spheroidal galaxies. Dark matter dominance is suggested.

Key words: stars: variables: other – stars: horizontal branch – galaxies: star clusters – globular clusters: general – galaxies: individual: Fornax dwarf spheroidal

1 INTRODUCTION

The Fornax dwarf galaxy is one of the most massive of the dwarf spheroidal (dSph) galaxies associated with the Milky Way (second only to the disrupted Sagittarius dSph), and the only undisturbed local galaxy to possess globular clusters (although Kleyna et al. (2003) have recently suggested the presence of a disrupted cluster in the Ursa Minor dSph). In this respect Fornax is somewhat unusual, because its population of five means that it has the highest specific frequency of globular clusters for any known galaxy.

As summarized by Strader et al. (2003), although small in number, this globular cluster system is remarkably complex. Buonanno et al. (1998b; 1999) have shown that clusters 1, 2, 3, and 5 appear coeval with both each other and the metal-poor galactic globular clusters, and that cluster 4 may be up to three gigayears younger. Strader et al. (2003) suggest that Fornax 5 may also be slightly younger. It has also been found (Smith et al. 1996; Buonanno et al. 1998b) that the Fornax globular clusters show evidence of the second parameter effect, whereby another parameter in addition to metallicity appears to define the morphology of the horizontal branch in a cluster. It is often assumed that age is the second parameter; however, if the age measurements listed above are correct,

* E-mail: dmackey@ast.cam.ac.uk

then it is possible that age is not the sole second parameter in the Fornax clusters. We (Mackey & Gilmore 2003b) have studied the surface brightness profiles of the Fornax globular clusters, and find a large amount of variation in the cluster structures – ranging from an extremely extended cluster (Fornax 1), to a strong post core-collapse candidate (Fornax 5). Evidently the Fornax cluster system is highly complicated; however both this complexity, and the system’s isolated nature provide unique opportunities for addressing the outstanding difficulties in our understanding of globular cluster formation and evolution. The Fornax globular clusters are therefore worthy of detailed study.

Much can be learned about a stellar population from the variable stars within that population, and given the relatively close proximity of the Fornax dwarf, it is perhaps surprising that a detailed investigation of stellar variability in its clusters has not been undertaken. In fact, we can find no quantitative identification and measurements of any variable stars in these objects in the literature – only several passing mentions of possible RR Lyrae detections exist (Buonanno et al. 1985; Demers et al. 1990; Buonanno et al. 1996; Smith et al. 1996; Smith et al. 1997; Buonanno et al. 1998b), along with one short article describing a survey in progress, and including cluster 3 (Maio et al. 2003).

In the process of obtaining photometry for colour-magnitude diagrams from archival *Hubble Space Telescope* observations, we noticed the possibility of surveying four of the Fornax globular clusters for RR Lyrae stars. We present here the results of this survey, which has been successful beyond our original expectations. We have discovered 197 RR Lyrae stars in the four clusters (Fornax 1, 2, 3, and 5), as well as 13 candidate horizontal branch variables. We describe the data and our survey strategy in Section 2, and present light curves and mean properties for each star in Section 3. Finally, we have been able to use the RR Lyrae discoveries to measure detailed information about each of the four clusters under consideration. This discussion is presented in Section 4.

2 OBSERVATIONS AND REDUCTIONS

2.1 Data

Wide Field Planetary Camera 2 (WFPC2) observations of four of the globular clusters in the Fornax dwarf galaxy (clusters 1, 2, 3, and 5, according to the notation of Hodge (1961)) are available in the *HST* archive (Program ID 5917). These observations were made between 1996 June 4 and 1996 June 6, through the F555W and F814W filters. The observational details are listed in Table 1.

Each cluster was imaged 14 times in F555W and 16 times in F814W, with individual exposure durations ranging from 160 – 600s, and 120 – 900s, respectively. Long total integration times are necessary because of the faintness of the Fornax globular clusters, which have distance moduli $(m - M)_0 \sim 20.68$ (Buonanno et al. 1999). The image sampling, presumably primarily intended to facilitate the removal of cosmic rays over the long integrations, renders the data suitable for identifying sources with short period variability, such as RR Lyrae stars. The exposure durations complement such identification, with horizontal branch (HB) stars being among the brightest stars in each image, and neither saturated nor overly faint in any image. Furthermore, observations through the two filters are interleaved, so that for any given F555W observation, it is possible to find an F814W image with a similar exposure duration and an observation date matching to ± 0.02 days. Such pairing of images allows colour information over a star’s variability cycle to be measured.

Although otherwise well suited for an RR Lyrae star search, the data have very short baselines of observation. This means that while variability can be easily detected, period determination is not straightforward – especially for RRab type variables, which typically have periods in the range 0.4 – 1.1 days. Unless such stars are fortuitously measured at a critical region of their light curve, the under-sampling renders accurate period determination virtually impossible. The shorter cycle RRc type variables, which have periods of 0.2 – 0.5 days, are more suited to the observation baselines. We will return to the question of period determination in Section 2.4.

Finally, we note that there also exist archival WFPC2 observations of Fornax cluster 4 (Program ID 5637). However, the data consist of only three images per filter, and given the significant crowding and field star contamination for this cluster, were not suitable for the present RR Lyrae work. We do not consider Fornax 4 further.

2.2 Photometry

All WFPC2 images we retrieved from the *HST* archive underwent preliminary reduction according to a standard pipeline, using the latest available calibrations. For photometric measurements from these calibrated images we used Dolphin’s HSTphot (Dolphin 2000a). This is a photometric package specifically designed for use on WFPC2 data. In particular, it uses a library of point spread functions (PSFs) tailored to account for the undersampled WFPC2 PSFs, allowing very accurate stellar centroiding and photometry.

Before running HSTphot, we completed several preprocessing steps. For each cluster, a reference image was identified (these are listed in Table 1) and all other images aligned with this image. This was achieved using the IRAF task IMALIGN, treating each image offset as a simple x - and y -shift. This is perfectly adequate for the present data – each image for a given cluster is offset from the reference image due to a simple dithering pattern of several pixels. There are no significant higher order distortions to account for.

Next, we used the utility software accompanying HSTphot to mask image defects (such as bad pixels and columns), calculate a background sky image (for use in the photometry calculations), and attempt to remove cosmic rays and unmasked hot-pixels. We then made photometric measurements on each image using HSTphot in PSF fitting mode (as opposed to aperture photometry mode). We set a minimum threshold for object detection of 3σ above the background. We also enabled two additional features of HSTphot. First, we elected to calculate a local adjustment to the background image before each photometry measurement, using the pixels just beyond the photometry radius (Dolphin 2000a). This helped account for regions of rapidly varying background, such as near the centres of the very crowded clusters 3 and 5. Second, we chose to run artificial star tests in conjunction with the photometry measurements. This option generates a large number of “fake” stars on a CMD, places them one at a time on the image, and solves each just as if it were a real star. This allows quantitative estimates of detection completeness as a function of a star’s magnitude, colour, and position in a cluster.

For each photometric measurement of a star (ideally, $14 \times$ F555W measurements and $16 \times$ F814W measurements) HSTphot output nine parameters, including flight magnitudes, standard magnitudes, and quantities characterizing the goodness-of-fit of the PSF solution (e.g., classification type, χ , S/N, and sharpness). Magnitudes from HSTphot are calibrated according to the recipe of

Table 1. WFPC2 observations of four of the globular clusters in the Fornax dwarf galaxy (Program ID 5917).

Cluster Name	Data-group F555W	Reference Image	Baseline (days)	N_{im}	Exposure Durations (s)	Data-group F814W	N_{im}	Exposure Durations (s)
Fornax 1	u30m010eb	u30m010et	0.3595	14	$3 \times 600s, 4 \times 500s, 3 \times 400s, 4 \times 160s$	u30m010ib	16	$2 \times 900s, 6 \times 700s, 2 \times 500s, 6 \times 120s$
Fornax 2	u30m020eb	u30m020et	0.3602	14	$3 \times 600s, 4 \times 500s, 3 \times 400s, 4 \times 160s$	u30m020ib	16	$2 \times 900s, 6 \times 700s, 2 \times 500s, 6 \times 120s$
Fornax 3	u30m030eb	u30m030et	0.3602	14	$3 \times 600s, 3 \times 500s, 3 \times 400s, 1 \times 378s, 4 \times 160s$	u30m030ib	16	$2 \times 900s, 6 \times 700s, 2 \times 500s, 6 \times 120s$
Fornax 5	u30m040eb	u30m040et	0.3553	14	$3 \times 600s, 4 \times 500s, 3 \times 400s, 4 \times 160s$	u30m040ib	16	$2 \times 900s, 6 \times 700s, 2 \times 500s, 6 \times 120s$

Holtzman et al. (1995), and using the latest updates of the Dolphin (2000b) CTE and zero-point calibrations. Each magnitude is corrected to a $0''.5$ aperture. HSTphot also provided mean positional information for each object, in the form of a chip number (where chip 0 refers to the PC, and chips 1 – 3 to WFC2-WFC4 respectively) and pixel coordinates relative to the frame of the reference image. These coordinates, in conjunction with the IRAF task METRIC and the cluster centres measured in Mackey & Gilmore (2003b), allowed us to calculate the radial distance of a given object from the centre of its cluster.

We used the goodness-of-fit parameters to select only objects with high quality photometry. We retained only measurements for which an object was classified as stellar (HSTphot types 1, 2, and 3), and for which $\chi \leq 2.5$, $S/N \geq 3.0$, $-0.3 \leq \text{sharpness} \leq 0.3$, and errors in the flight magnitude $\sigma_F \leq 0.1$. After the application of this filter, we kept only stars with five or more F555W-F814W pairs of successful measurements (where a pair is defined as two observations within ± 0.02 days of each other, as described in Section 2.1). We also passed the artificial star measurements through the quality filter. This allowed us to assign a detection completeness α_c to each real star, by finding the fraction of successful artificial star measurements in a brightness-colour-position bin about the real star. Bin widths were 0.25 mag in brightness, 0.2 mag in colour, and $2''$ in radial distance from the cluster centre. As an example, we consider a typical Fornax globular cluster RR Lyrae star, of magnitude $V = 21.3$, colour $V - I = 0.5$, and radial distance $r = 7''$. The fraction of successful artificial star measurements with $21.175 \leq V \leq 21.425$, $0.4 \leq V - I \leq 0.6$, and $6'' \leq r \leq 8''$ defines the detection completeness for this star. We expect the completeness values so derived to be accurate to a few per cent, except for very low fractions. Values of α_c less than ~ 0.25 should be regarded with caution.

2.3 Identification of Horizontal Branch variable stars

The completion of the photometry procedure resulted in a list of stars in each cluster, each with between 5 and 14 pairs of F555W and F814W measurements. In general, most stars possessed ~ 14 measurement pairs. Using colour-magnitude diagrams (CMDs) we selected stars in the HB region of each cluster, and determined the Welch & Stetson (1993) variability index I_{WS} for each. This index is calculated as follows. For N_o epochs of observations, each resulting in measurements $V_i \pm \sigma_{V,i}$ and $I_i \pm \sigma_{I,i}$, the weighted mean magnitudes

$$\bar{V} = \frac{\sum_{i=1}^{N_o} \frac{V_i}{\sigma_{V,i}^2}}{\sum_{i=1}^{N_o} \frac{1}{\sigma_{V,i}^2}} \quad \bar{I} = \frac{\sum_{i=1}^{N_o} \frac{I_i}{\sigma_{I,i}^2}}{\sum_{i=1}^{N_o} \frac{1}{\sigma_{I,i}^2}} \quad (1)$$

may be computed. The variability index is then defined as:

$$I_{WS} = \sqrt{\frac{1}{N_o(N_o - 1)}} \sum_{i=1}^{N_o} (\delta V_i \delta I_i) \quad (2)$$

where the normalized magnitude residuals are

$$\delta V_i = \frac{V_i - \bar{V}}{\sigma_{V,i}} \quad \delta I_i = \frac{I_i - \bar{I}}{\sigma_{I,i}} \quad (3)$$

The variability index therefore allows one to preferentially search for variations in photometric measurements which are correlated in the two colours being measured. For example, an RR Lyrae star will brighten and fade in both V and I , in *synchronization* over its pulsation cycle. Variability such as this results in a large value for I_{WS} . In the case of random errors – for example where one or more stellar images has been impacted by a cosmic ray, causing spurious variability in one colour band, or in the case where crowding introduces large random errors into each measurement – then δV_i and δI_i are uncorrelated, and the expectation value of I_{WS} is zero.

We therefore selected stars for which I_{WS} was greater than some positive constant as candidate variables. A small amount of experimentation showed $I_{WS} \geq 3.0$ to be a suitable value. The resultant candidate variable stars are shown in Fig. 1. We identified 283 candidates in total (24, 56, 137, and 66, in clusters 1, 2, 3, and 5, respectively). In each of the HB regions on the CMDs, the RR Lyrae strip is evident, and in most cases clearly defined on both edges. For each cluster, there also in general exist some candidate variable stars in the blue HB (BHB) region (except Fornax 1, for which no BHB extension is observed), and some along the red giant branch (RGB). Because we did not want to assume any information, a priori, about the exact limits of the instability strip on the HB, we tested all flagged variable stars equally as RR Lyrae candidates.

2.4 Light-curve fitting

The best way to identify a candidate star as an RR Lyrae, and in addition obtain quantitative information about its variability parameters, is to attempt to fit a light curve to its photometry. For very under-sampled data, such as the present measurements, this can be tricky. Eschewing elegance, the most reliable method is the simple application of brute force. We used a routine written by Andrew Layden (described in Layden & Sarajedini (2000); Layden et al.

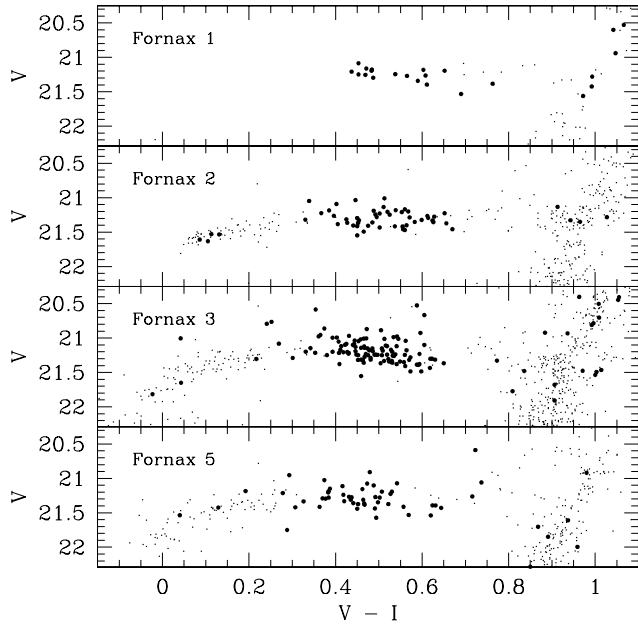


Figure 1. Colour-magnitude diagrams showing the horizontal branches of each of the four clusters. Stars with $I_{WS} \geq 3.0$ are marked as bold points – these are the candidate variables. The RR Lyrae region on each horizontal branch is well defined. We identified a total of 283 candidate variables – 24, 56, 137, and 66, in the four clusters respectively.

(1999); Layden (1998); and the references therein) for our period measurements.

This program works by taking a set of 10 variable star templates and attempting to fit them to the V -band photometric measurements for a number of different periods. The periods are selected by an incremental increase ΔP over a range P_1 to P_2 . For each candidate period, the measurements are folded, and a 3-parameter fit (magnitude zero-point, phase zero-point, and light-curve amplitude) made to each template. Six of the ten templates represent RRAb type variable stars, while two represent RRc type pulsators, and two represent variable binary stars (a W Ursae Majoris contact binary, and an Algol eclipsing binary). The RRAb curves (templates 1 – 6), and one of the RRc curves (template 7) are derived from high quality measured light curves, as described in Layden & Sarajedini (2000), and Layden (1998). The second RRc template (number 8) is a simple cosine curve. From each template fit, χ^2 is calculated. Period-template combinations with small χ^2 are likely to be the best representations of the measured data.

Such a procedure works well when the sampling is spread over a much longer baseline than the period of the variable star under consideration. In the present case however, our ~ 0.36 day baseline is in general *less* than one RR Lyrae pulsation cycle. For the short period (RRc) variables, which typically have $P < 0.45$ days, this does not pose too much of a problem. It is possible to derive a reliable period estimate for these stars, although naturally, accuracy would be greatly increased by having a baseline of many periods.

The situation is not so good for the RRAb variables, which might have periods typically about twice that of our baseline. It is possible to determine a reliable period estimate for such stars, but only under certain circumstances. Specifically, it is necessary to observe the full amplitude of a star’s variability (this allows the three parameters in a template fit to be well determined) and some

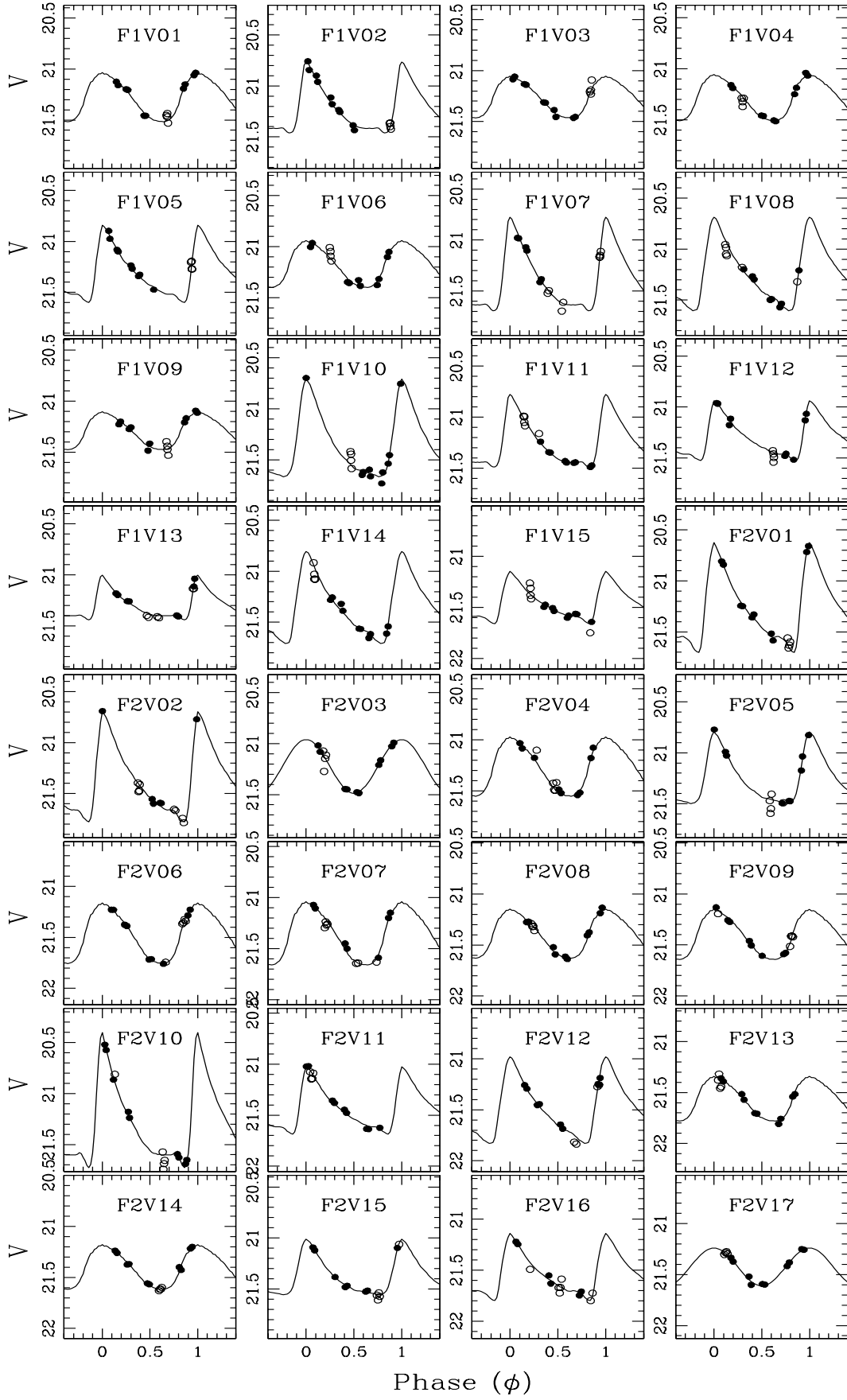
portion of its decline from maximum (which allows discrimination between different potential periods). For a mean RRAb period of 0.6 days (in which case our baseline is $0.6P$), examination of Figure 1 in Layden (1998) shows that we would observe the appropriate portion of the light curve in approximately ~ 40 per cent of cases. For shorter period RRAb stars this fraction is greater, and for longer period stars it is smaller. Another $\sim 10 - 20$ per cent of the time, we might observe *most* of the portion of the cycle which we require, in which case the derived period will be a good estimate. In the remainder of cases, without assuming some prior knowledge of either the star’s period or its amplitude, we cannot make an accurate period determination. In these incidences, we must make do with setting a lower limit to the period, which we achieve by assuming that the observed amplitude is the real amplitude of the star. The presence of these lower limits in our period measurements must be borne in mind if the data is put to any interpretive uses (see e.g., Section 4). Measurements at future epochs are required to pin down accurately the periods of such stars.

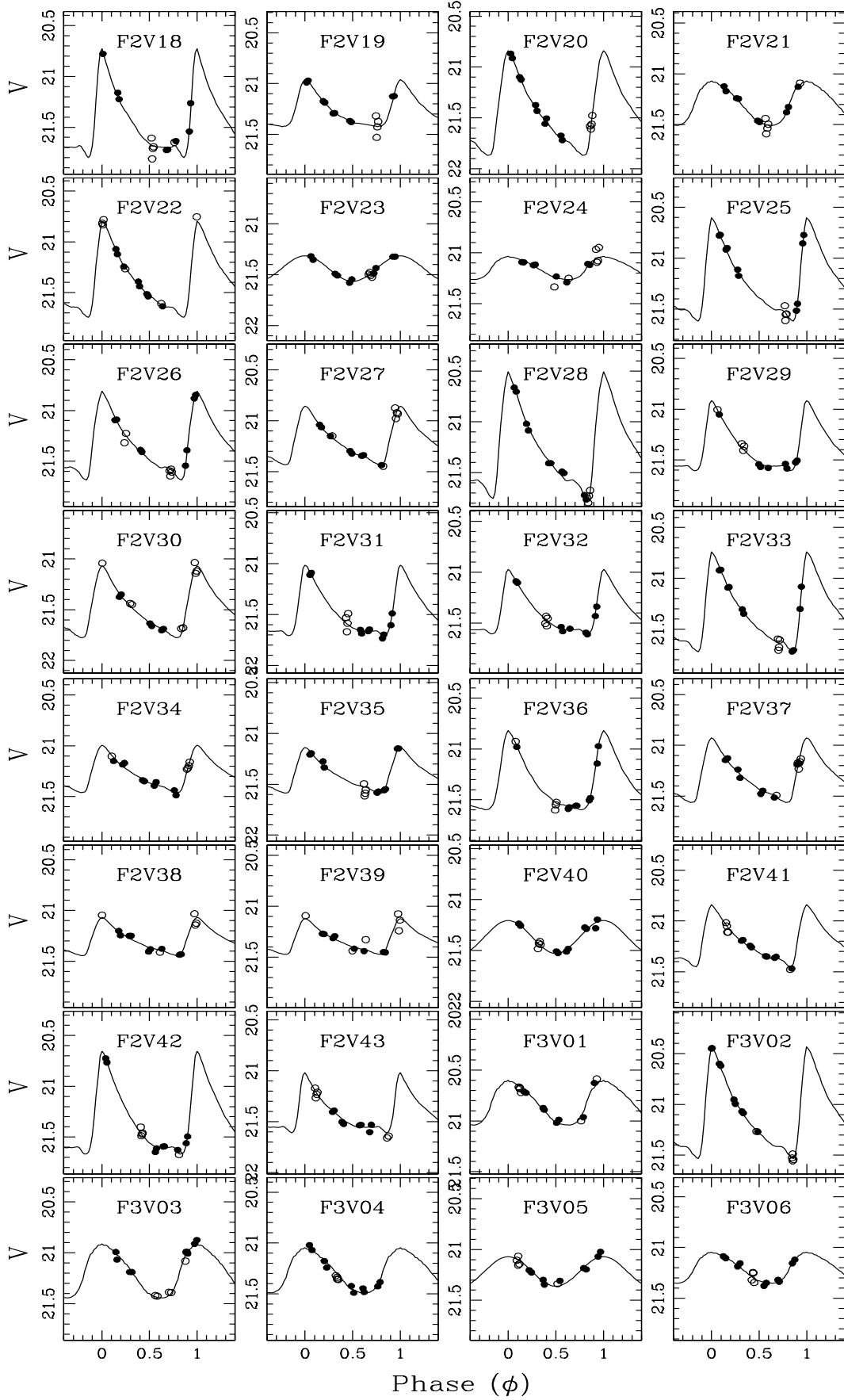
Since we were searching for RR Lyrae stars, we chose a period range of $0.2 - 1.0$ days, with $\Delta P = 0.01$ per cent. For each candidate, we examined the few fits to the V -band photometry with the smallest χ^2 . We used the I -band data as a consistency check, to verify that a fit which appeared suitable for the V -band photometry also resulted in a good I -band light-curve. In general the I -band data was of significantly poorer quality than the V -band data, so fitting templates directly to these measurements did not add useful information to the procedure. In the vast majority of cases, the V -band solution with the very smallest χ^2 provided evidently the best fit. We conservatively estimate the typical random uncertainty in any of our fitted periods to be ~ 0.005 days. While we identified plenty of RR Lyrae stars, we did not find any stars with data clearly best fit by either of the variable binary star templates. However, given our restriction to a small portion of the CMD, and our very short observation baseline, this is not too surprising. Most of the candidate variables flagged on the BHB or RGB seemed to have either poor measurements or some form of irregular variability. Certainly none had values of I_{WS} as large as those for typical RR Lyrae stars.

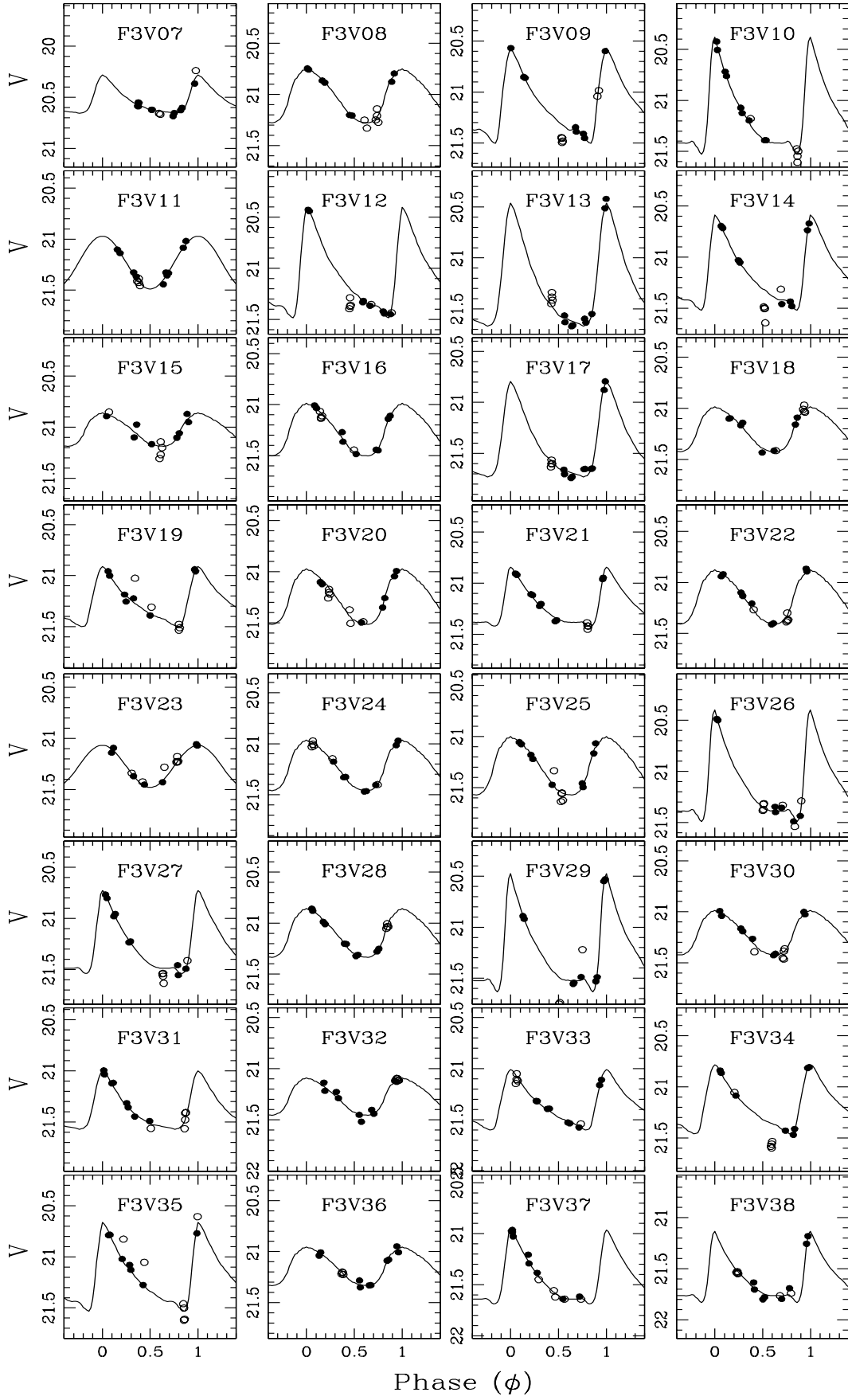
3 RESULTS

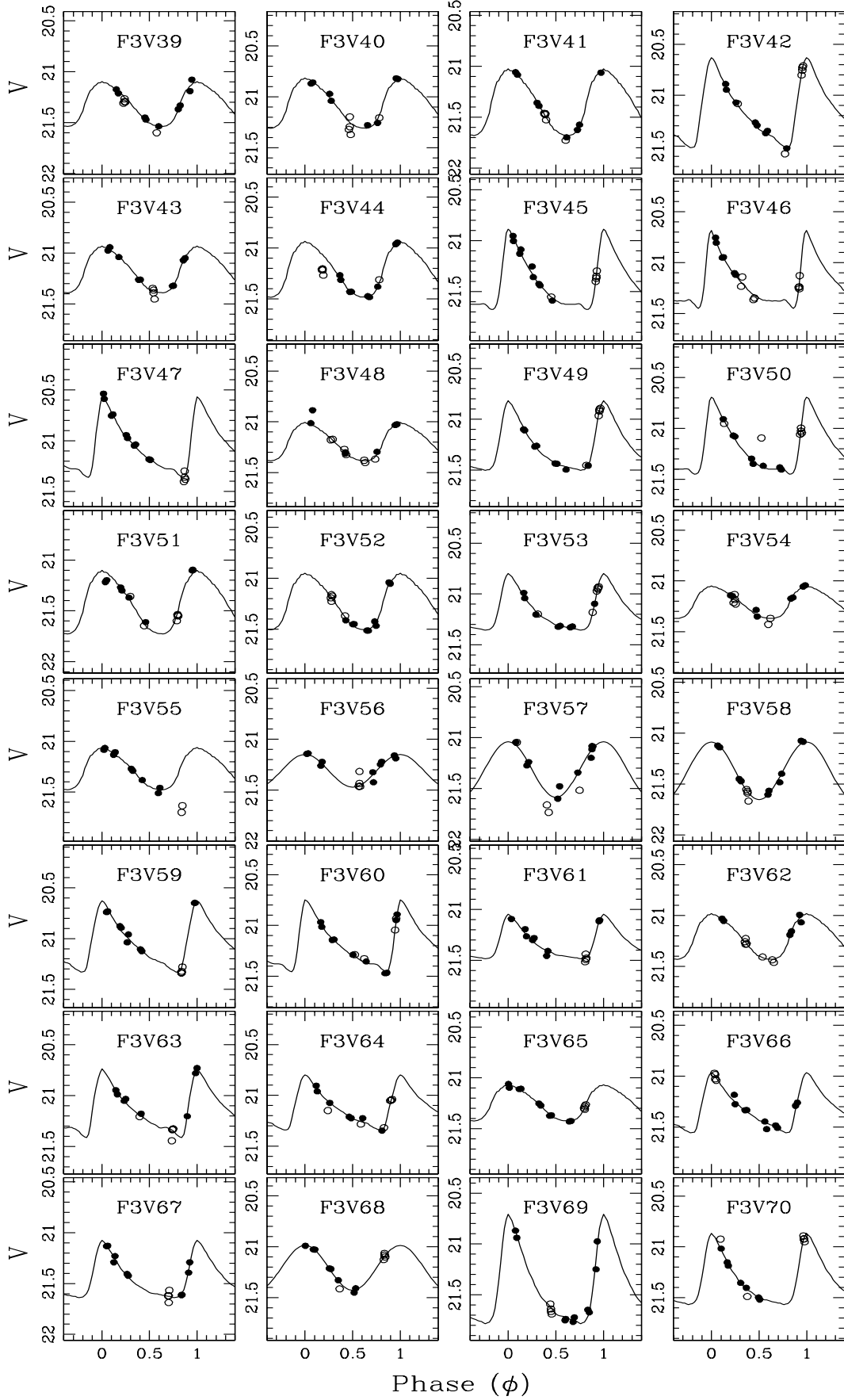
3.1 RR Lyrae stars

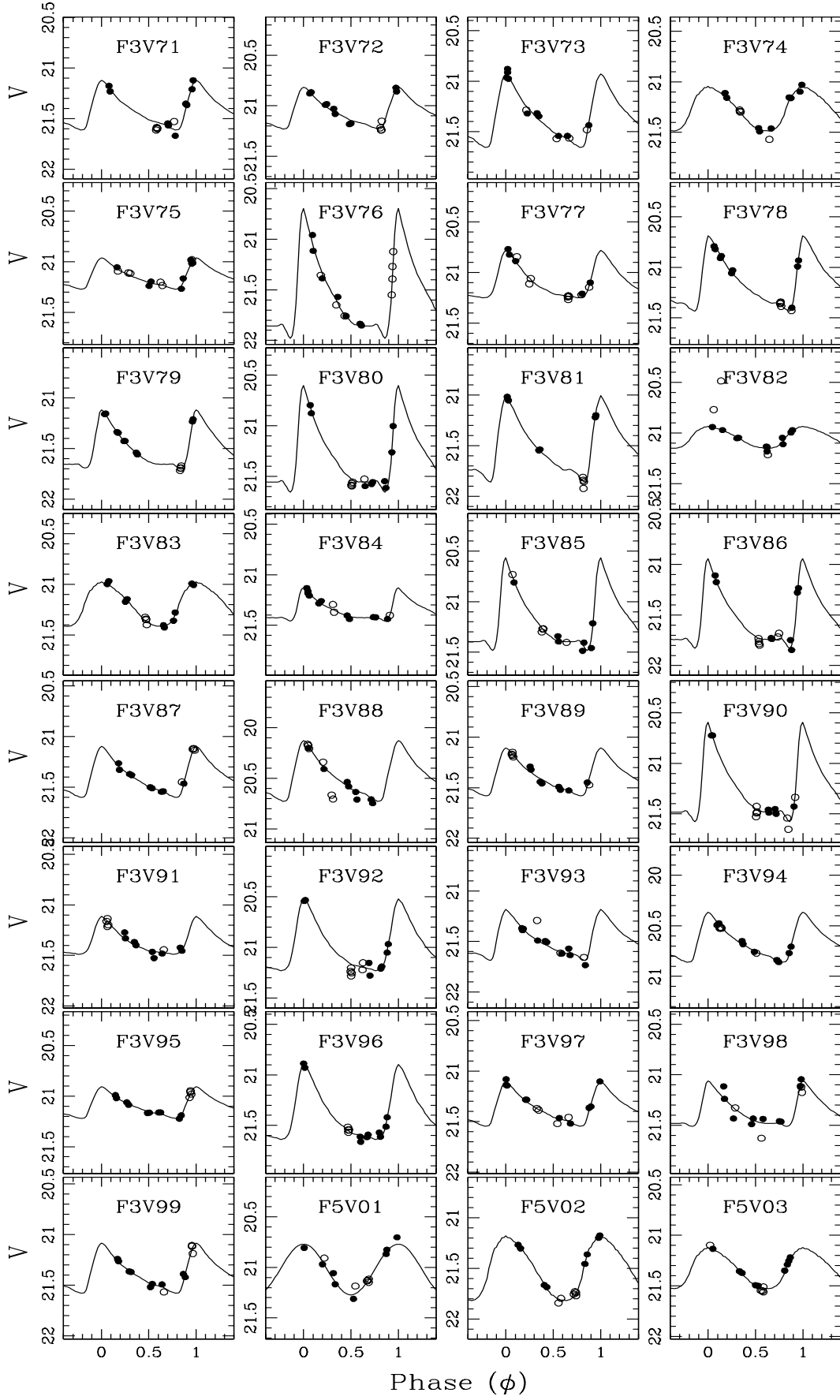
Of the 283 candidate objects, we identified 197 as RR Lyrae stars (15, 43, 99, and 40, in clusters 1, 2, 3, and 5, respectively). For each of these stars, we obtained template fits and period measurements. The best fitting V -band light curves are presented in Fig. 2, and the positions, periods, and fit parameters (template, rms scatter) listed in Table 2. In this table, the coordinates (chip, X_c , Y_c) are relative to the reference images listed in Table 1, and are in units of pixels. “Chip” refers to the camera on which the star was imaged – 0 is the PC, and 1 – 3 are WFC2–WFC4. The radii (r) and completeness fractions (α_c) are calculated as described in Section 2.2. N_t refers to the label of the best fitting template – numbers 1 – 6 are RRAb templates, and 7 – 8 are RRc templates. We consider periods marked with a star to be lower limit measurements. Note that on average, ~ 53 per cent of RRAb stars have periods which are not lower limits – in accordance with our estimate in Section 2.4. In addition, we have marked several stars with question marks next to their type. In these cases, the light curves were best fit by a template of the RR Lyrae type listed (i.e., RRAb or RRc), but could be fit by

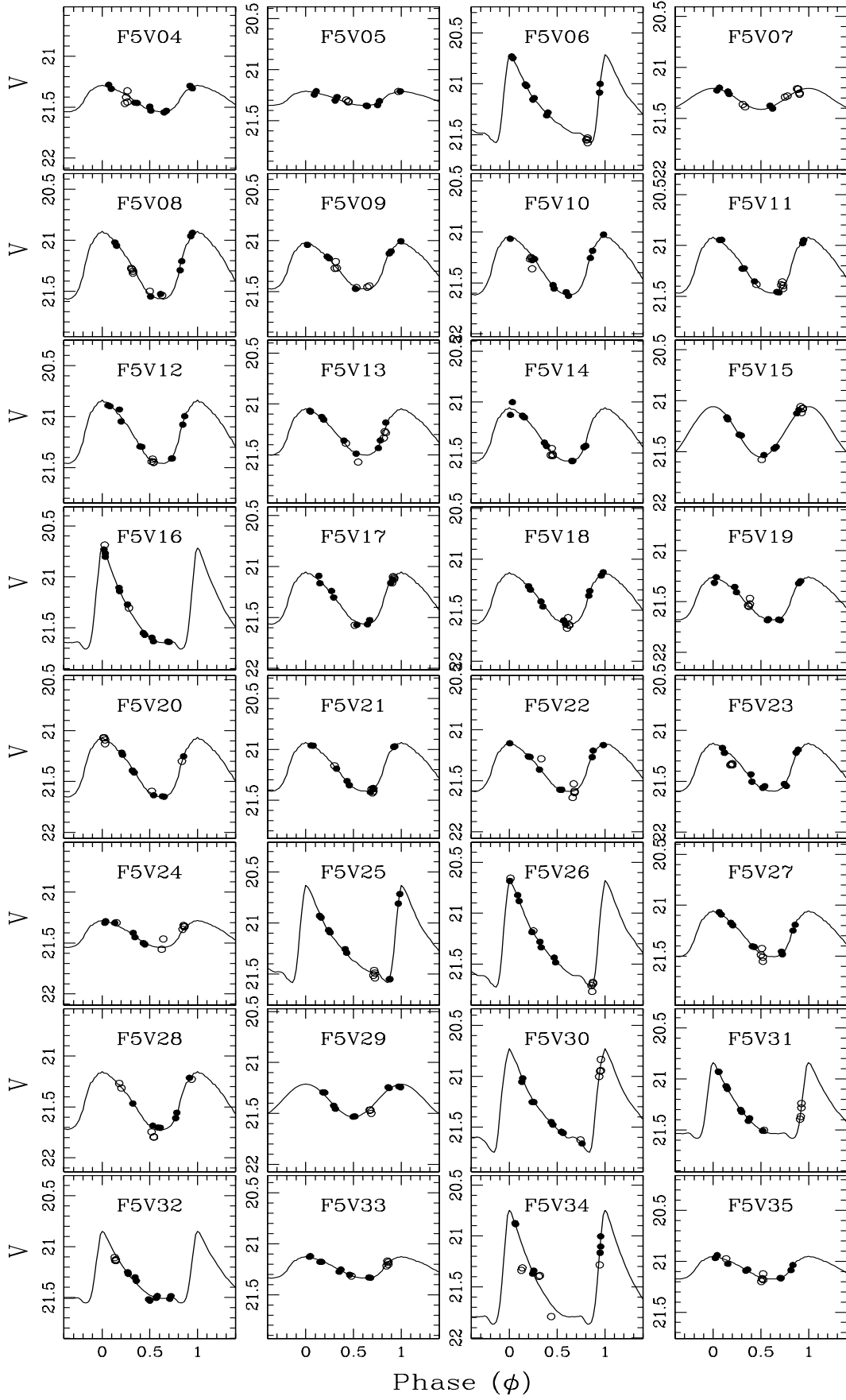












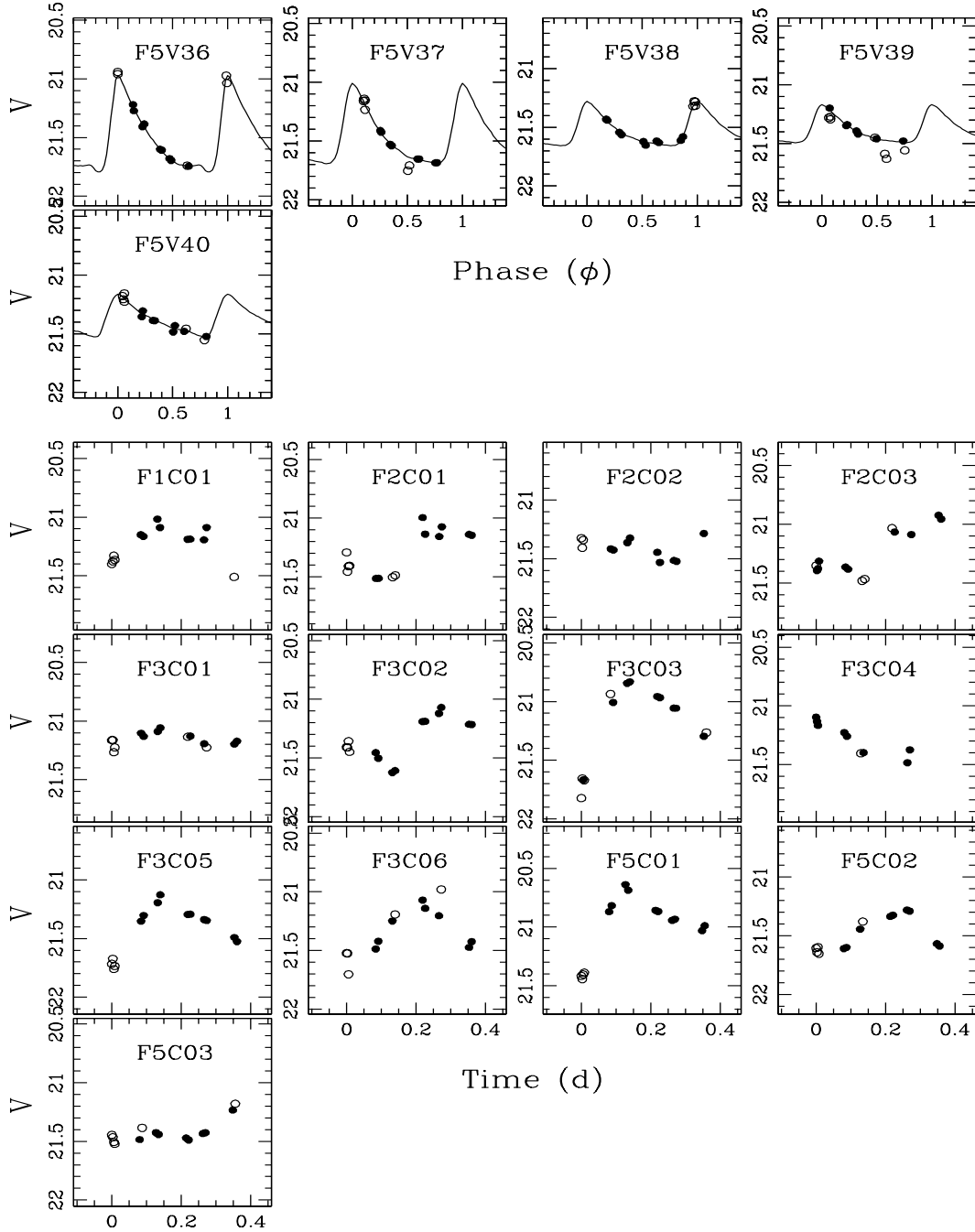


Figure 2. *V*-band photometric measurements and best fitting light-curves for the 197 RR Lyrae stars. In addition the *V*-band photometric measurements for the 13 candidate variable stars are plotted. In each plot, the hollow circles represent points which have measurement errors more than 1.5 times larger than the mean photometric error for observations of the given star. These usually represent the shortest duration exposures in each set. Typical measurement errors are just within the plotted points. This photometry is available on-line at http://www.ast.cam.ac.uk/STELLARPOPS/Fornax_RRLyr/.

a template of the other RR Lyrae type almost equally as well. Further measurements are required to confirm the listed classification for these stars.

It is clear from the α_c values that the only regions significantly affected by detection incompleteness are the very centres of the very crowded clusters 3 and 5. For cluster 3, completeness is significantly degraded within $\sim 4''$, and there are only two detections

within $2''$. Cluster 5 appears even more compact (cf. Mackey & Gilmore (2003b)), with completeness only degraded within $\sim 2''$; however, we note that there is only one detection within $1.5''$.

From the best fitting light curves, we computed an intensity mean *V* magnitude, denoted $\langle V \rangle$, and the maximum, minimum, and amplitude of the variability (V_+ , V_- , and ΔV , respectively). We note that these quantities are in general not significantly dif-

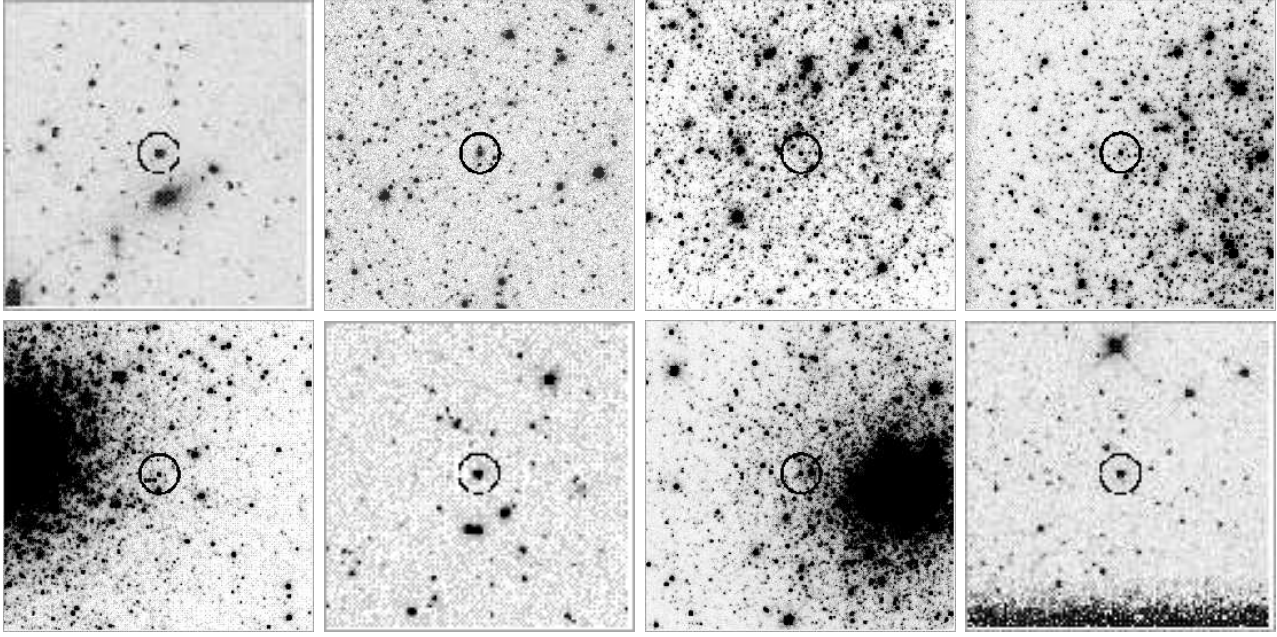


Figure 3. Example finder charts for eight of the RR Lyrae stars – two per cluster. From left to right: (top) F1V02, F1V14, F2V21, F2V28; (bottom) F3V42, F4V49, F5V06, F5V18. Each chart is $15''$ on a side. Three of the stars (F1V02, F3V49, and F5V18) are on WFC chips; the remainder are on the PC.

ferent from the same parameters derived directly from the V -band measurements. From the I -band measurements, we calculated the intensity mean $\langle I \rangle$. N_o is the number of pairs of observations for a given star. The parameter $^{\circ}E_m$ is the epoch of maximum, in days since MJD 50 000. The reader should bear in mind that this parameter is derived using a star's measured period. These quantities are all listed in Table 2.

We also characterized the colour of each RR Lyrae star. In accordance with Sandage (1990; 1993), we have calculated the magnitude mean of the N_o $(V - I)$ measurements per RR Lyrae to best represent the colour of an “equivalent static star”. This quantity, $\langle V - I \rangle$, is in preference to the two possible intensity mean colours $\langle V \rangle - \langle I \rangle$ and $\langle V - I \rangle$. Finally, the magnitude mean colour of an RR Lyrae star at its minimum light (defined to be phases $0.5 < \phi < 0.8$) can be of use (see Section 4.4). For stars with measurements falling in this phase range, we also calculated this colour (denoted $(V - I)_m$). Both colours are listed in Table 2, together with the calculated error σ_m in $(V - I)_m$, and the number of observations at minimum light N_m used in its calculation.

Finally, using the coordinates listed in Table 2, we constructed a finder chart for each RR Lyrae star. For reasons of practicality, we have not included the full set of charts in this paper; however, some examples are displayed in Fig. 3. The remainder are available from the author on request. Alternatively, they may be downloaded from http://www.ast.cam.ac.uk/STELLARPOPS/Fornax_RRLyr/ along with the light-curves, and data from Table 2.

3.2 Remaining candidates

In addition to these 197 objects, a further 13 stars fell within or nearby to the HB instability strip defined by the RR Lyrae stars. However, suitable template fits could not be obtained for these[†].

[†] This was generally because the shape of the variation did not match any of the templates, or because a template which fit in the V -band produced a

Plots of their photometry are presented at the end of Fig. 2. Most appear to have some form of cyclic variation, and given this and their locations on the HB, many are likely RR Lyrae stars of some sort. Their positions and completeness values are listed in Table 3, together with the photometric parameters $\langle V \rangle$, $\langle I \rangle$, V_+ , V_- , ΔV , and N_o . Unlike for the RR Lyrae stars, the V -band parameters for the present stars were of course calculated from the measured data. Finder charts are also available for these candidate RR Lyrae stars on-line, or by request.

3.3 Comparisons with previous work

Although we searched carefully, we were unable to find any published quantitative measurements of RR Lyrae stars in Fornax globular clusters. There has however been some work on the RR Lyrae population of the dwarf galaxy itself (e.g., Bersier & Wood (2002)). Nonetheless, several authors have noted the inevitable presence of RR Lyrae stars in the Fornax clusters, given their well populated horizontal branches, and on several occasions detections of variability have been made.

In one of the earliest CMD studies of the Fornax clusters, Buonanno et al. (1985) located several likely HB stars with variable photometry in their sample, and interpreted these as possible RR Lyrae stars. Buonanno et al. (1996) noted the presence of 17 horizontal branch stars with variable photometry in Fornax 1, and 40 such stars in Fornax 3. They identified these as RR Lyrae stars; however there were not enough measurements to obtain significant average magnitudes. Smith et al. (1996) detected 21 candidate HB variables in Fornax 1 based on a comparison of their photometry with that of Demers, Kunkel & Grondin (1990), who also found evidence for variability in a couple of HB stars. Similarly, Smith,

very poor light curve in the I -band. In many cases, the root cause is probably poor measurements due to crowding or other contamination, combined with genuine variability

Table 2. Measured and calculated properties of the RR Lyrae stars.

Name	Chip	X_c (pix)	Y_c (pix)	r ($''$)	α_c	Period (days)	Type	N_t	rms	$\langle V \rangle$	$\langle I \rangle$	$\overline{(V - I)}$	N_o	V_+	V_-	ΔV	$^\circ E_m$	$(V - I)_m$	σ_m	N_m
F1V01	1	206.81	310.88	43.50	1.00	0.459	RRc	7	0.016	21.275	20.822	0.452	14	21.034	21.516	0.482	237.4963	0.489	0.034	4
F1V02	1	383.22	130.61	29.80	1.00	0.570	RRab	3	0.030	21.206	20.687	0.492	14	20.765	21.460	0.695	237.8765	0.652	0.025	1
F1V03	3	118.48	282.34	26.11	1.00	0.425	RRc	7	0.015	21.261	20.798	0.450	14	21.055	21.465	0.410	237.4490	0.512	0.021	2
F1V04	3	209.32	86.92	35.78	1.00	0.396	RRc	7	0.017	21.281	20.794	0.495	14	21.054	21.508	0.454	237.6898	0.582	0.016	3
F1V05	1	410.36	122.48	30.62	1.00	0.589	RRab	2	0.026	21.285	20.697	0.503	13	20.842	21.599	0.757	237.2573	0.652	0.027	1
F1V06	0	464.51	285.29	8.00	1.00	0.440	RRc	7	0.026	21.169	20.691	0.483	14	20.939	21.399	0.460	237.6960	0.500	0.015	4
F1V07	0	586.78	766.38	17.53	1.00	0.580	RRab	3	0.039	21.348	20.690	0.576	14	20.775	21.693	0.918	237.2618	0.738	0.032	2
F1V08	0	709.54	616.83	16.99	1.00	0.465*	RRab	6	0.034	21.195	20.756	0.496	14	20.687	21.604	0.917	237.7498	0.598	0.017	4
F1V09	0	402.46	183.91	11.64	1.00	0.436	RRc	7	0.023	21.293	20.748	0.555	14	21.104	21.477	0.373	237.5112	0.569	0.040	4
F1V10	0	362.44	160.38	12.68	1.00	0.670	RRab	5	0.032	21.299	20.786	0.641	14	20.710	21.667	0.957	237.4937	0.715	0.018	5
F1V11	1	242.83	101.56	22.72	1.00	0.503*	RRab	3	0.011	21.228	20.716	0.562	14	20.777	21.488	0.711	237.7337	0.654	0.014	4
F1V12	0	587.09	652.50	13.52	1.00	0.644	RRab	2	0.019	21.287	20.619	0.664	13	20.940	21.525	0.585	237.4082	0.733	0.020	6
F1V13	3	132.83	53.26	30.19	1.00	0.424*	RRab?	1	0.012	21.290	20.673	0.592	14	21.002	21.442	0.440	237.4022	0.638	0.021	4
F1V14	0	379.05	321.76	5.34	1.00	0.460*	RRab	6	0.032	21.307	20.735	0.606	14	20.806	21.710	0.904	237.7688	0.704	0.016	4
F1V15	0	736.93	535.03	16.79	0.98	0.556*	RRab	4	0.022	21.444	20.802	0.700	14	21.147	21.659	0.512	237.6896	0.706	0.016	4
F2V01	0	386.68	480.06	2.25	0.96	0.429*	RRab	4	0.019	21.223	20.786	0.469	14	20.626	21.701	1.075	239.5524	0.620	0.021	6
F2V02	0	538.01	546.13	9.66	0.98	0.578	RRab	2	0.024	21.315	20.890	0.560	14	20.698	21.778	1.08	239.6668	0.662	0.015	6
F2V03	0	282.08	409.83	3.52	0.96	0.375	RRc	8	0.021	21.209	20.786	0.418	14	20.962	21.488	0.526	239.8160	0.411	0.016	4
F2V04	0	368.29	260.99	8.50	1.00	0.335	RRc	7	0.021	21.258	20.926	0.389	14	20.971	21.552	0.581	239.7316	0.479	0.017	4
F2V05	0	617.42	580.55	13.57	0.97	0.664	RRab	5	0.024	21.237	20.715	0.542	14	20.795	21.498	0.703	239.4942	0.610	0.017	8
F2V06	3	141.64	576.57	47.35	1.00	0.336	RRc	7	0.009	21.455	20.931	0.494	14	21.162	21.757	0.595	239.6009	0.693	0.021	3
F2V07	1	59.96	77.64	25.54	1.00	0.403	RRc	7	0.032	21.345	20.930	0.421	14	21.040	21.661	0.621	239.8042	0.516	0.018	4
F2V08	3	325.76	346.47	48.41	1.00	0.374	RRc	7	0.018	21.387	20.932	0.440	14	21.147	21.629	0.482	239.7992	0.529	0.022	2
F2V09	1	171.42	249.32	36.51	1.00	0.381	RRc	7	0.019	21.396	20.956	0.453	13	21.151	21.642	0.491	239.9604	0.500	0.017	4
F2V10	0	283.13	522.39	4.58	1.00	0.556	RRab	1	0.020	21.219	20.731	0.543	14	20.404	21.726	1.322	239.5312	0.612	0.029	5
F2V11	0	253.69	501.65	5.03	1.00	0.370*	RRab	2	0.023	21.416	20.796	0.506	13	21.026	21.686	0.660	239.8671	0.626	0.026	3
F2V12	0	656.24	746.22	19.36	0.97	0.354*	RRab?	6	0.026	21.455	20.950	0.477	13	20.981	21.831	0.850	239.5608	0.580	0.026	4
F2V13	3	183.13	764.91	65.34	1.00	0.345	RRc	7	0.020	21.561	21.061	0.467	14	21.341	21.779	0.438	239.8683	0.535	0.024	2
F2V14	1	219.03	428.71	53.86	1.00	0.404	RRc	7	0.020	21.399	20.964	0.463	14	21.179	21.617	0.438	239.6427	0.501	0.038	4
F2V15	0	442.63	313.64	7.39	0.97	0.403*	RRab	5	0.012	21.358	20.920	0.461	13	21.011	21.557	0.546	239.5840	0.501	0.021	6
F2V16	0	178.65	79.80	18.36	0.97	0.396*	RRab?	4	0.025	21.516	21.028	0.565	13	21.139	21.798	0.659	239.6814	0.594	0.033	6
F2V17	1	406.27	276.45	42.38	1.00	0.333	RRc	8	0.017	21.418	20.925	0.464	14	21.240	21.611	0.371	239.8469	0.487	0.014	4
F2V18	0	291.35	145.58	13.95	0.98	0.551	RRab	1	0.035	21.399	20.989	0.498	13	20.727	21.798	1.071	239.5952	0.605	0.021	8
F2V19	0	389.24	438.00	1.83	1.00	0.490*	RRab	5	0.022	21.256	20.736	0.511	14	20.960	21.423	0.463	239.5182	0.569	0.041	4
F2V20	0	366.18	412.15	1.75	1.00	0.514	RRab	6	0.018	21.405	20.765	0.617	14	20.840	21.870	1.030	239.4404	0.717	0.025	2
F2V21	0	391.94	407.81	2.61	0.97	0.387	RRc	7	0.014	21.289	20.811	0.520	14	21.069	21.507	0.438	239.6635	0.557	0.025	6
F2V22	0	168.22	625.25	11.54	1.00	0.567	RRab	2	0.014	21.344	20.655	0.544	14	20.797	21.744	0.947	239.8844	0.706	0.025	2
F2V23	3	54.41	232.32	19.43	0.97	0.337	RRc	8	0.014	21.436	20.942	0.510	14	21.315	21.565	0.250	239.6575	0.485	0.018	6
F2V24	0	538.69	384.36	9.05	0.98	0.389	RRc?	7	0.020	21.152	20.607	0.521	14	21.035	21.262	0.227	239.5243	0.541	0.023	3
F2V25	0	522.55	521.33	8.54	0.98	0.706	RRab	2	0.021	21.186	20.613	0.532	14	20.602	21.619	1.017	240.0444	0.632	0.044	4

Name	Chip	X_c (pix)	Y_c (pix)	r ($''$)	α_c	Period (days)	Type	N_t	rms	$\langle V \rangle$	$\langle I \rangle$	$\overline{(V - I)}$	N_o	V_+	V_-	ΔV	$^\circ E_m$	$(V - I)_m$	σ_m	N_m
F2V26	0	614.26	763.72	18.65	1.00	0.512	RRab	4	0.018	21.303	20.750	0.561	14	20.810	21.685	0.875	239.5189	0.785	0.049	4
F2V27	0	630.92	316.23	14.09	0.98	0.415*	RRab	6	0.010	21.184	20.591	0.566	14	20.854	21.433	0.579	239.4905	0.640	0.026	2
F2V28	0	206.64	518.13	7.27	0.97	0.366*	RRab	4	0.020	21.190	20.772	0.609	14	20.507	21.753	1.246	239.5796	0.608	0.024	3
F2V29	0	594.92	427.57	11.17	1.00	0.476*	RRab	3	0.025	21.353	20.841	0.571	12	20.916	21.604	0.688	239.7314	0.675	0.017	4
F2V30	0	736.48	463.22	17.55	1.00	0.414*	RRab	6	0.028	21.468	20.875	0.544	14	21.069	21.776	0.707	239.4791	0.663	0.018	4
F2V31	0	117.45	455.80	10.56	1.00	0.574	RRab	3	0.023	21.455	20.911	0.628	14	21.015	21.708	0.693	239.6350	0.625	0.018	4
F2V32	1	234.56	75.95	18.83	0.97	0.514	RRab	3	0.013	21.377	20.839	0.598	13	20.972	21.606	0.634	239.6824	0.653	0.017	3
F2V33	0	212.75	492.55	6.57	0.97	0.566	RRab	2	0.023	21.306	20.711	0.632	14	20.740	21.722	0.982	240.0546	0.755	0.050	4
F2V34	0	324.52	251.83	8.95	0.98	0.410*	RRab	6	0.025	21.263	20.695	0.572	14	20.996	21.461	0.465	239.9261	0.638	0.015	4
F2V35	3	82.59	311.95	24.90	1.00	0.624	RRab	6	0.020	21.396	20.808	0.602	14	21.139	21.586	0.447	239.4964	0.630	0.020	6
F2V36	0	325.10	654.98	9.51	0.98	0.602	RRab	5	0.027	21.307	20.788	0.576	13	20.819	21.600	0.781	239.5901	0.623	0.018	5
F2V37	0	284.47	544.16	5.33	1.00	0.357*	RRab?	6	0.034	21.287	20.645	0.625	14	20.927	21.563	0.636	239.5592	0.719	0.032	4
F2V38	0	375.04	424.16	1.54	1.00	0.423*	RRab	6	0.022	21.285	20.634	0.626	14	21.069	21.443	0.374	239.4710	0.678	0.018	3
F2V39	0	473.83	579.99	8.26	0.98	0.420*	RRab	6	0.019	21.326	20.666	0.633	14	21.122	21.474	0.352	239.4730	0.654	0.021	3
F2V40	2	376.04	267.21	62.42	1.00	0.445	RRc?	8	0.024	21.362	20.743	0.636	14	21.206	21.529	0.323	239.7434	0.715	0.016	4
F2V41	3	165.13	97.46	31.25	1.00	0.526	RRab	4	0.019	21.191	20.618	0.630	14	20.839	21.451	0.612	239.8026	0.665	0.014	4
F2V42	0	485.25	489.17	6.45	0.99	0.562	RRab	3	0.020	21.283	20.782	0.639	14	20.657	21.668	1.011	239.6534	0.661	0.015	5
F2V43	0	518.56	687.93	13.34	1.00	0.470*	RRab	1	0.028	21.403	20.767	0.671	14	21.018	21.611	0.593	239.8331	0.736	0.018	4
F3V01	0	336.08	534.52	5.13	1.00	0.334	RRc	7	0.028	20.822	20.553	0.235	14	20.602	21.041	0.439	238.8422	0.285	0.016	4
F3V02	0	353.43	332.31	4.80	1.00	0.562	RRab	2	0.010	21.062	20.585	0.457	14	20.435	21.533	1.098	238.4032	—	—	0
F3V03	0	410.86	470.41	2.07	0.90	0.321	RRc	7	0.027	21.176	20.822	0.308	14	20.911	21.445	0.534	238.5972	0.416	0.046	4
F3V04	1	113.33	98.49	25.28	1.00	0.303	RRc	7	0.027	21.270	20.974	0.348	14	21.047	21.491	0.444	238.7809	0.430	0.014	5
F3V05	0	432.93	526.50	4.78	0.86	0.311	RRc	8	0.030	21.211	20.828	0.348	14	21.071	21.361	0.290	238.8506	0.335	0.021	3
F3V06	0	535.69	539.75	8.39	1.00	0.312	RRc	7	0.017	21.201	20.846	0.382	14	21.045	21.352	0.307	238.7466	0.387	0.019	4
F3V07	0	341.33	445.33	2.07	0.75	0.589	RRab	5	0.026	20.522	20.240	0.329	14	20.281	20.655	0.374	238.6618	0.392	0.020	6
F3V08	0	394.59	462.39	1.41	0.20	0.301	RRc	7	0.024	21.011	20.659	0.383	14	20.748	21.277	0.529	238.6608	0.525	0.042	6
F3V09	0	373.71	572.11	6.35	1.00	0.580	RRab	4	0.013	21.093	20.618	0.534	14	20.568	21.502	0.934	238.5710	0.629	0.018	8
F3V10	0	421.96	348.88	4.18	1.00	0.528	RRab	1	0.018	21.095	20.591	0.517	14	20.380	21.526	1.146	238.4261	0.632	0.027	2
F3V11	0	466.71	440.11	3.73	0.90	0.277	RRc	8	0.022	21.215	20.931	0.359	14	20.972	21.488	0.516	238.7777	0.351	0.022	4
F3V12	0	404.05	518.93	4.00	1.00	0.620	RRab	2	0.015	21.021	20.652	0.578	14	20.403	21.484	1.081	238.6008	0.619	0.022	4
F3V13	0	206.01	302.14	10.08	1.00	0.627	RRab	5	0.038	21.189	20.793	0.557	13	20.463	21.669	1.206	238.6125	0.660	0.015	6
F3V14	0	421.69	596.34	7.61	0.89	0.479	RRab	2	0.018	21.126	20.690	0.487	14	20.587	21.520	0.933	238.6336	0.562	0.018	7
F3V15	0	432.78	450.30	2.31	0.81	0.298	RRc?	7	0.047	21.025	20.655	0.407	13	20.859	21.187	0.328	238.7009	0.453	0.029	6
F3V16	1	357.21	283.56	43.01	1.00	0.373	RRc	7	0.023	21.243	20.772	0.447	14	20.986	21.503	0.517	238.8264	0.489	0.016	3
F3V17	3	256.03	743.78	65.77	1.00	0.633	RRab	5	0.040	21.371	20.977	0.553	14	20.795	21.730	0.935	238.6126	0.638	0.013	6
F3V18	0	244.85	453.79	6.44	0.91	0.383	RRc	7	0.027	21.205	20.726	0.428	13	20.983	21.425	0.442	238.5250	0.520	0.024	2
F3V19	0	369.18	340.92	4.25	1.00	0.499*	RRab	6	0.031	21.246	20.732	0.475	13	20.912	21.499	0.587	238.4831	0.532	0.073	1
F3V20	0	360.55	481.99	2.49	0.81	0.383	RRc	7	0.019	21.242	20.796	0.451	14	20.972	21.516	0.544	238.7924	0.454	0.027	3
F3V21	0	397.75	561.52	5.87	1.00	0.526*	RRab	3	0.020	21.212	20.703	0.492	14	20.843	21.419	0.576	238.4591	0.620	0.083	1

Name	Chip	X_c (pix)	Y_c (pix)	r ($''$)	α_c	Period (days)	Type	N_t	rms	$\langle V \rangle$	$\langle I \rangle$	$\overline{(V - I)}$	N_o	V_+	V_-	ΔV	$^{\circ}E_m$	$(V - I)_m$	σ_m	N_m
F3V22	0	482.12	420.86	4.46	1.00	0.416	RRc	7	0.026	21.140	20.694	0.481	14	20.876	21.408	0.532	238.5678	0.568	0.019	6
F3V23	0	290.78	245.09	9.56	1.00	0.410	RRc	8	0.021	21.264	20.780	0.469	14	21.068	21.480	0.412	238.5615	0.493	0.022	6
F3V24	0	594.58	524.15	10.38	1.00	0.398	RRc	7	0.012	21.211	20.729	0.461	14	20.964	21.460	0.496	238.8566	0.588	0.017	4
F3V25	0	192.58	402.32	8.86	1.00	0.387	RRc	7	0.035	21.284	20.867	0.471	14	21.001	21.574	0.573	238.6752	0.471	0.021	6
F3V26	0	459.70	504.99	4.72	1.00	0.678	RRab	1	0.027	21.084	20.614	0.621	14	20.399	21.493	1.094	238.5383	0.629	0.019	8
F3V27	0	659.89	516.97	13.05	1.00	0.540	RRab	3	0.026	21.238	20.726	0.556	14	20.727	21.540	0.813	238.5400	0.594	0.021	6
F3V28	0	345.50	541.99	5.27	1.00	0.389	RRc	7	0.015	21.095	20.637	0.461	14	20.856	21.335	0.479	238.5543	0.500	0.017	4
F3V29	0	576.21	538.17	9.92	1.00	0.559	RRab	1	0.020	21.197	20.793	0.490	14	20.476	21.634	1.158	238.5992	0.614	0.020	7
F3V30	0	320.16	155.40	12.95	1.00	0.389	RRc	7	0.026	21.205	20.782	0.467	14	20.986	21.423	0.437	238.6022	0.510	0.020	6
F3V31	2	249.62	76.60	42.32	1.00	0.554*	RRab	5	0.025	21.363	20.779	0.546	13	20.999	21.572	0.573	238.9565	0.649	0.033	1
F3V32	1	179.45	98.61	23.14	1.00	0.360	RRc	7	0.029	21.274	20.762	0.472	14	21.090	21.455	0.365	238.5399	0.536	0.015	4
F3V33	3	210.24	410.88	39.41	1.00	0.401*	RRab?	6	0.012	21.346	20.824	0.476	14	21.010	21.601	0.591	238.8575	0.568	0.016	4
F3V34	0	399.75	324.37	4.99	1.00	0.568	RRab	6	0.009	21.166	20.656	0.567	13	20.784	21.460	0.676	238.5457	0.645	0.027	5
F3V35	0	342.01	458.86	2.28	0.81	0.607	RRab	2	0.048	21.168	20.617	0.477	14	20.664	21.532	0.868	238.3644	—	—	0
F3V36	0	476.83	661.28	11.17	1.00	0.460	RRc	7	0.021	21.146	20.672	0.491	14	20.954	21.334	0.380	238.7101	0.554	0.015	4
F3V37	0	426.12	503.72	3.72	0.80	0.495*	RRab	3	0.025	21.422	20.799	0.540	14	20.965	21.686	0.721	238.8745	0.637	0.028	4
F3V38	1	658.37	621.38	86.01	1.00	0.481*	RRab	1	0.032	21.581	21.057	0.546	14	21.132	21.830	0.698	238.7698	0.630	0.016	6
F3V39	3	209.41	689.64	58.73	1.00	0.380	RRc	7	0.032	21.318	20.827	0.495	14	21.096	21.539	0.443	238.7928	0.579	0.022	2
F3V40	0	368.42	380.44	2.51	0.81	0.441	RRc	7	0.024	21.061	20.562	0.530	13	20.815	21.309	0.494	238.6757	0.598	0.032	3
F3V41	0	96.81	294.20	14.51	1.00	0.380	RRc	7	0.017	21.346	20.912	0.507	13	21.024	21.682	0.658	238.7354	0.616	0.023	4
F3V42	0	545.33	407.93	7.38	0.91	0.425*	RRab	6	0.022	21.124	20.575	0.509	14	20.632	21.517	0.885	238.4765	0.636	0.016	4
F3V43	0	376.87	357.41	3.46	0.81	0.412	RRc	7	0.018	21.161	20.732	0.476	13	20.931	21.390	0.459	238.6587	0.483	0.026	6
F3V44	0	740.08	381.46	16.27	0.88	0.453	RRc	7	0.007	21.207	20.800	0.470	14	20.934	21.486	0.552	238.7992	0.515	0.023	4
F3V45	2	401.16	207.53	61.86	0.99	0.660	RRab	3	0.029	21.385	20.779	0.517	14	20.888	21.676	0.788	238.2720	—	—	0
F3V46	0	720.95	664.39	18.45	1.00	0.670	RRab	1	0.024	21.173	20.566	0.545	14	20.683	21.449	0.766	238.9354	—	—	0
F3V47	0	350.50	195.74	10.90	1.00	0.555	RRab	2	0.024	21.032	20.458	0.563	14	20.568	21.362	0.794	238.9554	0.644	0.025	1
F3V48	0	379.41	551.08	5.38	1.00	0.410	RRc	7	0.014	21.197	20.690	0.517	14	21.006	21.384	0.378	238.7094	0.613	0.040	4
F3V49	3	451.63	361.86	59.77	1.00	0.403*	RRab	5	0.015	21.249	20.694	0.502	13	20.818	21.503	0.685	238.8996	0.628	0.020	2
F3V50	0	379.45	557.58	5.67	1.00	0.447*	RRab?	3	0.025	21.170	20.669	0.468	14	20.692	21.449	0.757	238.9094	0.516	0.019	4
F3V51	0	94.20	588.37	14.94	1.00	0.535	RRc?	7	0.042	21.409	20.851	0.528	14	21.103	21.728	0.625	238.4568	0.547	0.058	3
F3V52	1	780.06	396.32	75.82	1.00	0.576	RRc?	7	0.019	21.225	20.801	0.512	14	20.949	21.508	0.559	238.7226	0.548	0.013	6
F3V53	0	517.90	431.75	6.05	0.91	0.367*	RRab?	5	0.015	21.153	20.621	0.500	14	20.798	21.356	0.558	238.5377	0.603	0.015	4
F3V54	0	403.01	484.67	2.49	0.81	0.364	RRc	7	0.024	21.212	20.715	0.488	14	21.049	21.369	0.320	238.7943	0.662	0.035	2
F3V55	0	528.34	369.69	7.13	0.91	0.466	RRc	7	0.015	21.270	20.826	0.474	11	21.060	21.477	0.417	238.4885	0.587	0.023	2
F3V56	0	297.03	330.07	6.16	0.91	0.585	RRc?	8	0.030	21.305	20.760	0.524	14	21.151	21.472	0.321	238.5482	0.535	0.018	7
F3V57	0	477.99	779.51	16.24	1.00	0.408	RRc?	8	0.049	21.297	20.748	0.556	14	21.041	21.588	0.547	238.5237	0.503	0.025	4
F3V58	0	99.56	359.59	13.38	1.00	0.381	RRc	8	0.023	21.352	20.899	0.508	14	21.087	21.655	0.568	238.7387	0.562	0.017	4
F3V59	0	490.48	706.09	13.27	1.00	0.613	RRab	6	0.031	21.024	20.433	0.561	14	20.630	21.330	0.700	238.3681	—	—	0
F3V60	0	202.59	472.21	8.48	1.00	0.394*	RRab	2	0.019	21.163	20.607	0.550	14	20.747	21.455	0.708	238.5063	0.620	0.020	4
F3V61	0	562.75	509.53	8.80	1.00	0.590	RRab	5	0.026	21.329	20.783	0.533	13	21.048	21.485	0.437	238.4022	—	—	0

Name	Chip	X_c (pix)	Y_c (pix)	r ($''$)	α_c	Period (days)	Type	N_t	rms	$\langle V \rangle$	$\langle I \rangle$	$\overline{(V - I)}$	N_o	V_+	V_-	ΔV	$^\circ E_m$	$(V - I)_m$	σ_m	N_m
F3V62	0	338.62	432.19	2.11	0.81	0.463	RRc	7	0.024	21.208	20.694	0.514	13	20.982	21.432	0.450	238.7159	0.637	0.057	3
F3V63	0	320.81	404.73	3.19	0.81	0.531*	RRab	4	0.024	21.122	20.544	0.564	13	20.735	21.411	0.676	238.4886	0.633	0.061	4
F3V64	0	243.38	328.13	8.01	1.00	0.385*	RRab?	6	0.023	21.108	20.584	0.555	13	20.799	21.341	0.542	238.5344	0.569	0.023	2
F3V65	0	294.80	572.98	7.57	0.91	0.416	RRc	7	0.011	21.249	20.732	0.526	14	21.067	21.425	0.358	238.5482	0.553	0.028	3
F3V66	2	75.95	275.55	44.77	1.00	0.412*	RRab	6	0.030	21.303	20.742	0.512	14	20.967	21.557	0.590	238.8661	0.585	0.015	4
F3V67	3	98.01	707.04	54.71	1.00	0.618	RRab	5	0.027	21.433	20.831	0.595	14	21.075	21.639	0.564	238.4486	0.756	0.049	4
F3V68	0	279.88	332.29	6.62	0.91	0.510	RRc	8	0.017	21.197	20.642	0.542	13	20.987	21.428	0.441	238.9672	0.613	0.026	2
F3V69	3	103.09	149.54	23.75	0.91	0.555	RRab	5	0.044	21.363	20.822	0.639	14	20.709	21.784	1.075	238.6336	0.689	0.016	4
F3V70	0	207.17	481.52	8.38	1.00	0.664	RRab	5	0.025	21.308	20.625	0.539	13	20.867	21.569	0.702	238.9016	0.699	0.031	1
F3V71	2	481.32	510.67	87.41	1.00	0.701	RRab	6	0.031	21.403	20.852	0.581	14	21.122	21.612	0.490	238.4729	0.642	0.015	8
F3V72	0	332.84	570.22	6.67	0.89	0.523*	RRab	6	0.027	21.055	20.458	0.590	14	20.817	21.229	0.412	238.4555	—	—	0
F3V73	0	400.86	340.76	4.26	1.00	0.415*	RRab	6	0.037	21.337	20.706	0.580	14	20.929	21.654	0.725	238.8752	0.713	0.036	4
F3V74	0	220.40	692.51	13.93	1.00	0.412	RRc	7	0.028	21.266	20.705	0.564	13	21.046	21.485	0.439	238.7453	0.672	0.022	4
F3V75	0	382.96	385.97	2.14	0.81	0.391*	RRab?	6	0.024	21.142	20.575	0.542	14	20.962	21.271	0.309	238.5093	0.582	0.035	4
F3V76	2	126.87	746.74	90.31	1.00	0.528	RRab	1	0.049	21.489	20.819	0.625	14	20.697	21.980	1.283	238.3870	0.694	0.039	2
F3V77	0	478.84	443.13	4.30	1.00	0.590	RRab	5	0.025	21.082	20.476	0.599	14	20.781	21.252	0.471	238.4935	0.632	0.048	5
F3V78	0	238.81	426.41	6.66	0.91	0.721	RRab	2	0.020	21.126	20.549	0.557	14	20.689	21.434	0.745	239.0515	0.646	0.038	4
F3V79	3	364.46	109.74	49.93	1.00	0.655	RRab	3	0.012	21.485	20.858	0.572	14	21.117	21.691	0.574	238.9895	—	—	0
F3V80	1	276.06	192.60	32.34	1.00	0.621	RRab	1	0.042	21.265	20.757	0.624	14	20.602	21.657	1.055	238.5658	0.638	0.015	8
F3V81	0	53.44	643.37	17.76	0.88	0.657	RRab	4	0.020	21.488	20.970	0.504	10	21.006	21.859	0.853	238.3446	—	—	0
F3V82	0	443.58	442.36	2.70	0.81	0.509	RRc	7	0.019	21.046	20.501	0.500	14	20.935	21.150	0.215	238.5657	0.518	0.024	6
F3V83	0	295.07	466.47	4.37	1.00	0.444	RRc	7	0.020	21.197	20.676	0.545	14	20.975	21.416	0.441	238.6740	0.639	0.019	4
F3V84	0	419.13	367.98	3.34	0.80	0.312*	RRab?	1	0.018	21.345	20.716	0.596	14	21.128	21.457	0.329	238.8683	0.630	0.034	2
F3V85	0	437.33	355.86	4.24	1.00	0.509*	RRab	1	0.040	21.148	20.691	0.560	12	20.567	21.483	0.916	238.6852	0.632	0.020	3
F3V86	2	539.43	80.14	69.02	1.00	0.648	RRab	1	0.036	21.504	20.949	0.632	14	20.942	21.828	0.886	238.5342	0.686	0.023	8
F3V87	0	358.82	594.17	7.42	1.00	0.397*	RRab	6	0.017	21.386	20.753	0.587	14	21.097	21.601	0.504	238.4966	0.666	0.017	4
F3V88	1	647.16	88.87	47.12	1.00	0.524*	RRab	6	0.029	20.469	19.968	0.498	14	20.128	20.728	0.600	238.8568	0.595	0.015	4
F3V89	0	282.57	458.47	4.80	1.00	0.440*	RRab	6	0.027	21.379	20.737	0.616	13	21.107	21.580	0.473	238.8521	0.669	0.021	3
F3V90	0	434.05	379.93	3.29	0.81	0.664	RRab	1	0.026	21.214	20.755	0.597	14	20.593	21.577	0.984	238.5428	0.551	0.022	8
F3V91	0	432.48	394.74	2.78	0.80	0.453*	RRab	5	0.033	21.356	20.727	0.616	14	21.115	21.488	0.373	238.8540	0.637	0.019	4
F3V92	0	343.88	428.18	1.89	0.04	0.688	RRab	5	0.027	20.968	20.408	0.670	14	20.523	21.231	0.708	238.5377	0.705	0.023	7
F3V93	1	645.48	496.28	74.83	1.00	0.536*	RRab	4	0.026	21.476	20.851	0.653	14	21.183	21.688	0.505	238.7887	0.670	0.029	4
F3V94	0	712.80	327.71	15.62	1.00	0.362*	RRab?	6	0.011	20.650	20.061	0.587	14	20.367	20.861	0.494	238.8351	0.677	0.014	3
F3V95	0	473.68	389.27	4.50	0.88	0.394*	RRab	6	0.014	21.090	20.421	0.652	14	20.907	21.221	0.314	238.9062	0.669	0.016	3
F3V96	1	219.83	284.31	41.08	1.00	0.659	RRab	5	0.029	21.361	20.816	0.633	14	20.896	21.638	0.742	238.5711	0.629	0.014	5
F3V97	0	478.20	456.30	4.37	0.82	0.397*	RRab	6	0.024	21.361	20.652	0.661	14	21.110	21.545	0.435	238.4847	0.717	0.028	4
F3V98	0	552.32	766.78	16.89	1.00	0.451*	RRab	3	0.057	21.351	20.669	0.646	14	21.062	21.508	0.446	238.4394	0.692	0.027	4
F3V99	0	502.74	389.31	5.72	0.82	0.383*	RRab	6	0.031	21.368	20.695	0.649	13	21.083	21.580	0.497	238.5170	0.722	0.019	4
F5V01	0	420.01	498.13	2.69	0.99	0.405	RRc	8	0.041	21.007	20.676	0.345	14	20.771	21.272	0.501	237.9404	0.471	0.025	6

Name	Chip	X_c (pix)	Y_c (pix)	r ($''$)	α_c	Period (days)	Type	N_t	rms	$\langle V \rangle$	$\langle I \rangle$	$\overline{(V - I)}$	N_o	V_+	V_-	ΔV	$^\circ E_m$	$(V - I)_m$	σ_m	N_m
F5V02	0	91.38	247.48	16.23	0.96	0.311	RRc	7	0.009	21.493	21.199	0.343	14	21.179	21.819	0.640	237.9882	0.433	0.032	6
F5V03	0	445.78	401.77	3.43	0.95	0.278	RRc	7	0.009	21.326	21.049	0.320	14	21.121	21.528	0.407	238.0563	0.410	0.027	5
F5V04	3	64.07	311.29	22.53	0.91	0.315	RRc	7	0.019	21.418	21.041	0.378	14	21.284	21.545	0.261	238.1354	0.413	0.017	3
F5V05	0	347.30	687.40	10.96	1.00	0.394	RRc	7	0.015	21.284	20.920	0.367	13	21.211	21.351	0.140	238.0430	0.384	0.017	4
F5V06	0	277.07	471.31	5.10	0.98	0.595	RRab	2	0.011	21.215	20.631	0.536	14	20.713	21.577	0.864	237.7311	—	—	0
F5V07	0	290.49	593.95	7.91	1.00	0.300	RRc	8	0.017	21.306	20.904	0.377	14	21.205	21.412	0.207	237.9470	0.329	0.020	4
F5V08	0	391.59	375.00	3.37	0.99	0.419	RRc	7	0.023	21.237	20.848	0.410	14	20.911	21.578	0.667	238.0836	0.532	0.026	3
F5V09	0	349.28	424.61	2.04	0.99	0.378	RRc	7	0.014	21.247	20.836	0.400	13	21.016	21.477	0.461	238.0961	0.545	0.025	4
F5V10	0	422.69	317.87	6.18	1.00	0.340	RRc	7	0.020	21.325	20.915	0.401	14	21.038	21.619	0.581	238.1377	0.536	0.026	2
F5V11	0	325.60	391.00	3.84	0.99	0.364	RRc	7	0.018	21.191	20.786	0.451	14	20.919	21.468	0.549	237.9517	0.548	0.023	6
F5V12	2	323.81	545.98	81.04	1.00	0.396	RRc	7	0.025	21.143	20.743	0.465	14	20.838	21.459	0.621	238.0049	0.551	0.021	6
F5V13	0	396.96	424.02	1.22	0.39	0.368	RRc	7	0.026	21.273	20.846	0.439	14	21.044	21.501	0.457	237.9100	0.509	0.027	4
F5V14	0	380.64	327.69	5.53	1.00	0.372	RRc	7	0.028	21.317	20.899	0.469	14	21.055	21.583	0.528	238.0498	0.518	0.020	3
F5V15	0	465.75	515.87	4.70	1.00	0.362	RRc	8	0.016	21.291	20.828	0.425	14	21.058	21.552	0.494	237.8789	0.568	0.017	4
F5V16	0	405.52	290.88	7.24	1.00	0.520	RRab	3	0.014	21.332	20.792	0.436	14	20.716	21.708	0.992	238.2011	0.554	0.017	4
F5V17	0	554.79	363.72	8.56	1.00	0.353	RRc	7	0.022	21.310	20.870	0.397	14	21.055	21.566	0.511	237.8923	0.544	0.034	4
F5V18	1	385.96	81.77	25.97	1.00	0.361	RRc	7	0.015	21.382	20.960	0.475	14	21.131	21.635	0.504	237.9931	0.558	0.019	6
F5V19	3	378.12	714.40	71.86	1.00	0.404	RRc	7	0.023	21.47	20.995	0.486	14	21.256	21.681	0.425	238.0630	0.570	0.018	4
F5V20	0	694.33	577.77	15.10	1.00	0.422	RRc	7	0.011	21.356	20.914	0.416	14	21.068	21.652	0.584	238.2059	0.573	0.019	4
F5V21	0	417.89	512.44	3.21	0.94	0.351	RRc	7	0.010	21.171	20.748	0.482	14	20.931	21.412	0.481	237.9694	0.552	0.025	6
F5V22	0	468.89	628.90	8.97	1.00	0.402	RRc	7	0.016	21.367	20.905	0.482	14	21.129	21.605	0.476	237.9445	0.577	0.022	6
F5V23	1	476.49	152.30	37.03	1.00	0.379	RRc	7	0.033	21.362	20.91	0.459	14	21.126	21.599	0.473	238.1427	0.476	0.017	4
F5V24	0	437.65	424.47	2.56	0.99	0.445	RRc	7	0.015	21.413	20.934	0.452	14	21.278	21.543	0.265	237.8350	0.456	0.034	2
F5V25	0	463.33	340.50	6.04	1.00	0.494	RRab	2	0.020	21.18	20.685	0.521	14	20.630	21.584	0.954	237.8604	0.517	0.050	4
F5V26	0	227.21	589.26	9.66	0.98	0.571	RRab	2	0.016	21.28	20.712	0.538	14	20.680	21.726	1.046	237.7202	—	—	0
F5V27	0	432.85	616.59	7.89	1.00	0.382	RRc	7	0.014	21.281	20.837	0.489	14	21.055	21.506	0.451	238.0194	0.518	0.021	6
F5V28	0	115.32	737.13	17.89	0.95	0.326	RRc	7	0.021	21.434	21.073	0.454	13	21.152	21.722	0.570	238.0419	0.471	0.020	8
F5V29	0	471.83	291.22	8.15	1.00	0.420	RRc	8	0.019	21.367	20.874	0.501	13	21.212	21.534	0.322	237.9307	0.602	0.038	4
F5V30	3	211.47	345.73	37.21	1.00	0.433*	RRab	4	0.019	21.297	20.728	0.518	14	20.730	21.746	1.016	238.2367	0.644	0.015	4
F5V31	0	437.38	321.31	6.25	1.00	0.572	RRab	3	0.012	21.31	20.706	0.557	14	20.841	21.582	0.741	237.6900	0.682	0.029	2
F5V32	0	347.33	243.78	9.51	1.00	0.603	RRab	3	0.032	21.296	20.794	0.534	14	20.850	21.553	0.703	238.1314	0.573	0.016	5
F5V33	0	293.43	457.39	4.28	1.00	0.428	RRc?	7	0.011	21.234	20.685	0.538	14	21.125	21.337	0.212	238.2763	0.591	0.021	2
F5V34	0	326.89	674.77	10.60	1.00	0.720	RRab	3	0.049	21.433	20.74	0.490	13	20.747	21.864	1.117	238.2507	—	—	0
F5V35	0	351.30	494.77	2.64	0.94	0.415	RRc?	7	0.014	21.066	20.547	0.536	14	20.951	21.174	0.223	238.0014	0.539	0.023	6
F5V36	3	501.81	655.42	77.55	1.00	0.540	RRab	3	0.016	21.488	20.804	0.559	14	20.971	21.792	0.821	237.6789	0.674	0.023	2
F5V37	0	378.58	336.97	5.11	0.98	0.532*	RRab	5	0.015	21.441	20.923	0.551	14	21.009	21.696	0.687	238.1578	0.640	0.015	6
F5V38	0	336.72	619.27	8.06	0.98	0.392*	RRab	5	0.015	21.524	20.86	0.627	14	21.279	21.659	0.380	237.8331	0.656	0.017	4
F5V39	0	616.54	781.25	18.24	1.00	0.513*	RRab	5	0.017	21.378	20.836	0.542	14	21.168	21.493	0.325	238.1786	0.636	0.031	4
F5V40	0	418.38	479.85	2.00	0.95	0.466*	RRab	6	0.021	21.373	20.746	0.617	14	21.163	21.527	0.364	238.1904	0.627	0.017	5

Table 3. Photometric measurements for the candidate RR Lyrae stars.

Name	Chip	X_c	Y_c	r	α_c	$\langle V \rangle$	$\langle I \rangle$	N_o	V_+	V_-	ΔV
F1C01	2	216.99	73.27	39.27	1.00	21.356	20.796	13	21.017	21.510	0.493
F2C01	0	270.89	750.76	14.21	0.98	21.253	20.729	14	20.995	21.514	0.519
F2C02	0	181.01	437.51	7.69	0.97	21.395	20.877	12	21.286	21.533	0.247
F2C03	0	494.90	97.50	17.17	1.00	21.164	20.577	13	20.924	21.482	0.558
F3C01	0	292.15	545.72	6.64	1.00	21.143	20.802	14	21.057	21.266	0.209
F3C02	0	102.44	473.52	12.95	1.00	21.318	20.825	14	21.069	21.625	0.556
F3C03	0	355.77	453.05	1.61	0.08	21.326	20.851	14	20.832	21.823	0.991
F3C04	0	425.88	793.12	16.40	0.88	21.316	20.714	9	21.097	21.484	0.387
F3C05	3	498.62	616.54	74.58	1.00	21.496	20.878	14	21.127	21.760	0.633
F3C06	0	386.76	392.09	1.86	0.12	21.375	20.679	13	20.980	21.704	0.724
F5C01	0	471.40	480.74	4.10	0.98	21.076	20.557	14	20.639	21.444	0.805
F5C02	0	121.56	309.44	13.62	1.00	21.519	20.984	14	21.281	21.653	0.372
F5C03	0	492.01	202.26	12.19	0.98	21.350	20.785	14	21.180	21.522	0.342

Rich & Neill (1997) found evidence for 7 HB variables in Fornax 3, and one variable above the Fornax 3 HB. Using the WFPC2 data from the present study, Buonanno et al. (1998b) identified 8, 39, 66, and 36 candidate RR Lyrae stars in clusters 1, 2, 3, and 5, respectively, based on the fact that these stars had frame-to-frame variations greater than 3σ . These numbers are quite similar to ours, as might be expected given that we are using the same observations. However, we detect more RR Lyraes in all clusters, demonstrating the sensitivity of our search strategy.

More recently, Maio et al. (2003) have described wide-field observations of a region of the Fornax dwarf, including cluster 3. They detect 70 candidate variables in a $95'' \times 95''$ box centred on this cluster, most of which lie on the HB. This is again fewer variables than we detect in Fornax 3; however, the present WFPC2 observations have superior resolution to the terrestrial wide-field observations. Maio et al. (2003) present preliminary uncalibrated light curves for two of their candidate cluster 3 RR Lyraes; however neither these nor any of their other variables are identified, and no quantification of the variability is presented.

We therefore believe that all of the 197 RR Lyrae stars and 13 candidates we describe here have been newly identified. This is the first time that calibrated light curves and variability data have been published for any RR Lyrae stars in the globular clusters in the Fornax dwarf galaxy.

3.4 Effects of under-sampling

We consider briefly here the effects that our short baselines of observation are expected to have on the RR Lyrae parameters derived from the fitted light curves. As described in Sections 2.4 and 3.1, the primary effect is that ~ 50 per cent of the calculated RRab periods are lower limits. This has knock-on effects for most of the other quantities computed for these stars, which must be accounted for if any use is to be made of the measurements (e.g., in determining distance moduli).

For example, suppose an RRab star has a true amplitude $(\Delta V)_t = (V_-)_t - (V_+)_t$ and a true period of pulsation P_t . However, because of our limited baseline of observation ($< P_t$), we have only measured $\Delta V < (\Delta V)_t$ for this star, and hence determined a period $P < P_t$ (as described in Section 2.4). This will lead to a systematic error in our calculation of $\langle V \rangle$ from the fitted light curve. It is possible that we have sampled only the brightest portion of the light curve, so that our measurement of V_+ is accurate, but

in this case our assumed V_- will be brighter than $(V_-)_t$ and our calculated $\langle V \rangle$ will also be brighter than the true intensity-mean V magnitude $\langle V \rangle_t$. Similarly, it is possible that we have accurately measured V_- , but assumed too faint a value for V_+ . In this case our $\langle V \rangle$ will be fainter than $\langle V \rangle_t$. For symmetric light curves, such systematic errors should average to zero over a large ensemble of stars; however RRab stars have significantly asymmetric pulsations, in that they are brighter than $\langle V \rangle_t$ for typically only $\sim 30 - 40$ per cent of a cycle. Hence, while determinations of $\langle V \rangle$ for each star individually may be either too bright or too faint, we expect on average that our measurements will provide values of $\langle V \rangle$ somewhat fainter than $\langle V \rangle_t$ (i.e., we measure V_- accurately more often than we measure V_+ accurately). The same reasoning applies for calculations involving $\langle I \rangle$, which are made directly from the photometry.

For stars with lower limit periods, our measurement of the magnitude-mean colour over the cycle will also suffer a systematic error. Because we will have preferentially sampled the RRab light curves around minimum light, on average a measurement of $\langle V - I \rangle$ will be redder than its true value, because minimum light is the reddest part of the pulsation cycle. We note that individual measurements may, of course, also be too blue – this is just more unlikely than a red error.

It is more complicated to estimate the effect of a lower-limit period on a measurement of $(V - I)_m$. Only points with phases in the range $0.5 < \phi < 0.8$ are used in the calculation of this parameter. Since we have $P < P_t$, the true phase of any given point will be smaller than the phase calculated using P . Hence, it is likely that we have used points which have true phases $\phi_t < 0.5$ in our calculations, and that on average our measured $(V - I)_m$ values will be too blue. We note that this effect will be small, since the rate of change of colour around the minimum of an RRab pulsation cycle is slow.

There are two ways to account for these systematic errors if any use of the derived data is made – for example, in determining the distance modulus to Fornax. The first is simply to leave the stars flagged as having lower limit periods out of the calculations. Alternatively, it is possible just to use those stars which have large amplitudes (say $\Delta V > 0.9$), since these are the most likely to have an accurate determination for P . These two methods allow a consistency check to be made, and the magnitude of any of the systematic errors described above to be investigated.

4 DISCUSSION

Because the RR Lyrae populations of the Fornax globular clusters have not been previously investigated in a quantitative manner, it is useful to consider their characteristics. Much can be learned from the measurements we have made, even bearing in mind the uncertainties in the period fitting. As discussed in Section 3.4, it is possible to investigate and account for the systematic errors our procedure might introduce. Throughout the following Sections, Table 4 keeps a record of the calculations we discuss.

4.1 Specific frequencies

Each of the four Fornax clusters we have examined has a significant population of RR Lyrae stars. To investigate this quantitatively we calculate the RR Lyrae specific frequency, S_{RR} , which is the number of RR Lyrae stars in a cluster normalized to a cluster absolute magnitude of $M_V = -7.5$:

$$S_{RR} = N_{RR} 10^{0.4(7.5+M_V)} \quad (4)$$

Buonanno et al. (1998b) have noted that S_{RR} for Fornax clusters 1, 2, 3, and 5 appears quite high relative to the Milky Way globular clusters.

We calculate S_{RR} using the integrated luminosities for the four Fornax clusters derived by us from accurate surface brightness profiles (Mackey & Gilmore 2003b). For the four clusters we obtained integrated luminosities $\log(L_\infty/L_\odot) = 4.07, 4.76, 5.06$, and 4.76 respectively. These correspond to F555W luminosities. Assuming the F555W solar magnitude to be $V_{555}^\odot = +4.85$ (Mackey & Gilmore 2003a), we obtain absolute magnitudes of $-5.33, -7.05, -7.80$, and -7.05 for the four clusters. These are in good agreement with the values derived by Buonanno et al. (1985), and the values listed by Webbink (1985).

The specific frequencies for the four clusters are then $S_{RR} = 110.7, 65.1, 75.1$, and 60.5 , respectively. We note that these are lower limits, because we have not included information about detection completeness, or counted the candidate variable stars. We can account for completeness effects using the α_c values in Table 2. To avoid unwarranted weighting by the few stars with very low completeness fractions, we set any α_c values of less than 0.25 equal to 0.25. If we then assume that all the candidate variable stars are actually RR Lyrae stars, we obtain specific frequencies of $S_{RR} = 118.2, 70.5, 90.2$, and 68.4 . These are still lower limits, because in no cases did the WFPC2 observations cover an entire cluster. Hence, the samples of RR Lyrae stars are certainly incomplete, but in calculating S_{RR} , we have normalized the N_{RR} values to *full cluster* luminosities. Accounting for this effect is not trivial, because we do not know the spatial distribution of RR Lyrae stars in any cluster, and because the WFPC2 geometry is complicated. Given that we have imaged the centre of each cluster, we expect the N_{RR} to be 80 – 90 per cent complete. Hence, the S_{RR} values may be 10 – 20 per cent greater than quoted above.

These specific frequencies are extremely high compared to those for the galactic globular clusters. The catalogue of Harris (1996) lists only four of the ~ 150 galactic clusters as having $S_{RR} > 60$, and only two of these have $S_{RR} > 100$. The largest value, that for Palomar 13, is $S_{RR} = 127.5$. Given our sample incompleteness, it is very likely that Fornax 1 has S_{RR} significantly greater than this. It is certainly intriguing that only a tiny fraction of galactic globular clusters have very high S_{RR} , whereas *all* of the Fornax clusters we have investigated do – this is a fact worthy of further attention.

4.2 Oosterhoff classification

It is also instructive to investigate the relationship between the derived periods and amplitudes for our RR Lyrae populations. This can be done by plotting a period-amplitude diagram for each cluster. For galactic globular clusters, such diagrams fall naturally into two distinct groups – the Oosterhoff type-I and type-II clusters (OoI and OoII, respectively). Each group has characteristic properties, summarized in Smith (1995). Furthermore, there is in general a close relationship between period and amplitude for the RRab stars in a cluster – namely that the shortest period RRab stars have the largest amplitudes, while those with the smallest amplitudes have the longest periods.

Period-amplitude diagrams for the four Fornax clusters are presented in Fig. 4. RRab stars with good periods are plotted as filled circles, while those with lower limit periods are plotted as crosses. RRc stars are plotted as triangles – those with uncertain classification in Table 2 are hollow points, while the remainder are filled. From examination of these diagrams, evidence of the lower limit period problem is immediately clear. The crosses form a distinct population between the good RRab stars and the RRc stars in each diagram. Once good periods are determined for these stars, they will move into the regions occupied by the good RRab stars. In the best populated clusters, such as Fornax 3, evidence of the upper part of the RRab sequence can be seen, although the relationships certainly have significant scatter. Improved period measurements should tighten these sequences.

From the period-amplitude diagrams it is not possible to determine conclusively whether the Fornax clusters resemble either the OoI or OoII clusters, or (like the old LMC clusters and several dwarf spheroidal galaxies) have properties which lie somewhere in between the two (e.g., Pritzl et al. (2002)). We can shed some light on this by calculating selected parameters for each of our RR Lyrae populations. Smith (1995) lists the OoI clusters as having $\langle P_{ab} \rangle = 0.55$ d, $\langle P_c \rangle = 0.32$ d, and $N_c/N_{RR} = 0.17$, and the OoII clusters as having $\langle P_{ab} \rangle = 0.64$ d, $\langle P_c \rangle = 0.37$ d, and $N_c/N_{RR} = 0.44$. Pritzl lists these parameters for several old LMC clusters. These have $\langle P_{ab} \rangle = 0.56 - 0.60$ d, $\langle P_c \rangle = 0.33 - 0.38$ d, and $N_c/N_{RR} = 0.3 - 0.5$, placing them in general somewhere between the OoI and OoII groups.

We calculated these parameters for the four Fornax clusters – the results are listed in Table 4. Our $\langle P_c \rangle$ values cover the range 0.37–0.43 d, which are similar to those for OoII clusters. However, excepting Fornax 5, the fraction N_c/N_{RR} ranges from 0.3 – 0.38 for the Fornax clusters, which is more similar to the intermediate LMC clusters than either of the Oosterhoff groups. Given the presence of the many RRab stars with lower limit periods, it does not make sense for us to calculate $\langle P_{ab} \rangle$ using all our RRab stars[†]. It is far more useful to calculate this quantity using only those RRab stars with good periods. If we do this, we obtain values in the range 0.57 – 0.61, again most similar to the intermediate LMC clusters. We must bear in mind however that these averages do not include many stars with long periods, since we have only measured lower limit periods for these stars. Hence, these mean values will likely increase once all stars have good periods.

One final discriminator we can use is the transition period P_{tr} of RRab stars – that is, the shortest period that this class of stars have in a given cluster, without being RRc stars. Given the inverse period-amplitude relation for RRab stars, those with the

[†] although we list this value in Table 4 for comparative purposes.

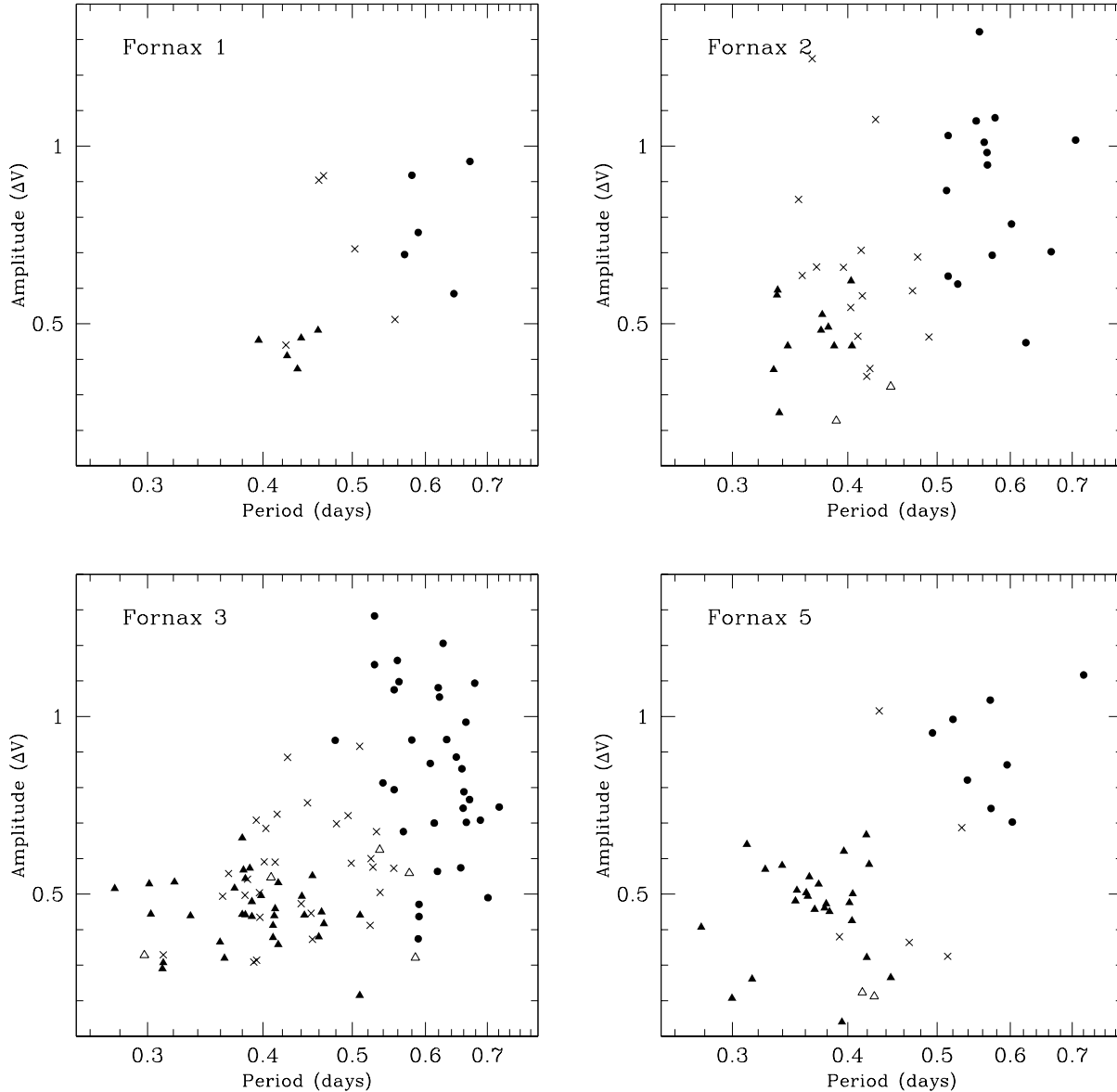


Figure 4. Period-amplitude diagrams for each of the four clusters. RRab stars with good periods are plotted as solid circles; those with lower limit periods are crosses. RRc stars with uncertain classification are hollow triangles, while the remainder are solid triangles.

shortest periods have the largest amplitudes. Calculating $\langle P_{ab} \rangle$ for our RRab stars with $\Delta P > 0.9$ therefore provides a good estimate of P_{tr} . Smith (1995) lists $P_{tr} = 0.43$ for OoI clusters and $P_{tr} = 0.55$ for OoII clusters. Our values range from $0.54 - 0.58$, which match the OoII clusters well.

Hence we can rule out the possibility that the Fornax globular clusters 1, 2, 3, and 5 resemble the galactic OoI type clusters. However, with quite a dispersion in their properties, it is not clear whether they do resemble either the OoII type clusters, or the intermediate LMC type clusters. Both N_c/N_{RR} and $\langle P_{ab} \rangle$ suggest an intermediate-type classification, while $\langle P_c \rangle$ and P_{tr} suggest a similarity to the OoII clusters. One explanation is that the Fornax clusters are, like the LMC clusters, of intermediate classification, but with somewhat different characteristics. This interpretation is consistent with the observation that the properties of RR Lyrae stars measured in the *fields* of dwarf galaxies classify these objects also

as intermediate, but with a considerable range in properties (see e.g., Pritzl et al. (2002)). Bersier & Wood (2002) have measured the properties of the field RR Lyrae population in Fornax, and find $\langle P_{ab} \rangle = 0.585$ and a mean RR Lyrae $[\text{Fe}/\text{H}] \sim -1.8^{\S}$. This metallicity is very similar to those for Fornax clusters 2 and 5 (see Section 4.6 and Table 4), which also have $\langle P_{ab} \rangle \sim 0.58$. Clusters 1 and 3 are somewhat more metal poor, with $[\text{Fe}/\text{H}] \sim -2$, and have slightly longer mean RRab periods – $\langle P_{ab} \rangle \sim 0.61$. From the list in Pritzl, these are most similar to the Carina and Draco dwarf galaxies, which also have $[\text{Fe}/\text{H}] \sim -2$, and $\langle P_{ab} \rangle \sim 0.62$. In fact,

[§] In fact, they measure $[\text{Fe}/\text{H}] \sim -1.6$ on the Butler-Blanco metallicity scale, which is ~ 0.2 dex more metal rich than the Zinn & West (1984) scale. We quote the metallicity on the latter scale for consistency with the measurements in Table 4.

the Carina RR Lyrae stars have recently been studied in detail by Dall'Ora et al. (2003), who find that $\langle P_{ab} \rangle$ for these stars matches well the OoII clusters, but that N_c/N_{RR} matches the OoI clusters – a similar situation to that for the Fornax clusters. These combinations are the strongest indicators that the Fornax globular clusters also deserve an intermediate Oosterhoff classification.

4.3 The strange case of Fornax 5

It is worth commenting briefly on cluster 5, which has somewhat exceptional properties. Specifically, it has a very large relative population of RRc stars, so that $N_c/N_{RR} = 0.68$. This is significantly larger than any of the RR Lyrae populations listed in the compilation of Pritzl et al. (2002), in which the largest belongs to the LMC cluster NGC 2257, with $N_c/N_{RR} = 0.50$.

The period-amplitude diagram for Fornax 5 is also unusual, in that in addition to the well defined RRab and RRc groups, there appears a third group of four stars in the very lower left of the diagram. This group strongly resembles the putative RRe type stars (second overtone pulsators) identified by Clement & Rowe (2000) in ω Centauri. Although there has been some debate in the literature over the existence (or not) of such objects, there have been several instances of observational evidence (see the references in Clement & Rowe). The ~ 20 RRe candidates identified by Clement & Rowe have a mean period of 0.304 days, and a range 0.28 – 0.35 days. The four candidates in Fornax 5 (F0503, F0504, F0505, and F0507) have a range 0.28 – 0.39 days, and a mean of 0.32 days. The mean amplitude of the ω Cen objects is slightly larger than 0.2 mag, which also matches the mean amplitude of the Fornax 5 candidates: $\langle \Delta V \rangle \sim 0.25$ mag. Hence the two groups of stars occupy the same region on the period-amplitude diagram, and we conclude that the four Fornax 5 objects are good RRe candidates. We note that these four stars are among the five bluest RR Lyrae stars in this cluster, adding weight to the argument. There also exist several similar stars in clusters 2 and 3; however these do not seem as well separated on the period-amplitude diagrams as the cluster 5 stars, and we cannot claim them as RRe candidates with certainty.

Returning to the question of the large number of RRc stars in Fornax 5, even subtracting the four potential RRe stars from the calculation leaves $N_c/N_{RR} = 0.58$ – still an unusually large value. It is interesting to note that Fornax 5 is unique in additional ways – it is in the very outer regions of the Fornax dwarf, and it is the only post core-collapse candidate in the system (Mackey & Gilmore (2003b)). It seems difficult to imagine some link between the structure of the cluster and its RR Lyrae star population however, especially given that neither ω Cen nor NGC 2257 are exceptionally compact objects.

4.4 Reddening towards the Fornax globular clusters

It is a well known property of ab-type RR Lyrae stars that they have extremely similar intrinsic colours at minimum light, independent of metallicity: $[(V - I)_m]_0 = 0.58 \pm 0.03$ (see e.g., Mateo et al. (1995) and references therein). This can be used to determine the line-of-sight reddening to a group of RRab stars. The validity of this technique has been demonstrated for RR Lyrae stars in the Sagittarius dwarf galaxy by both Mateo et al. (1995) and Layden & Sarajedini (2000).

To apply this technique to the four Fornax clusters individually, we calculated the weighted mean $\langle (V - I)_m \rangle$ for each sample of RRab stars, using the $(V - I)_m$ and σ_m measurements from

Table 2. We obtained $\langle (V - I)_m \rangle = 0.68 \pm 0.01$ for Fornax 1, 0.65 ± 0.01 for Fornax 2, 0.63 ± 0.01 for Fornax 3, and 0.62 ± 0.01 for Fornax 5. To investigate the possibility of systematic errors due to the lower limit periods, as described in Section 3.4, we recalculated these values – first using only RRab stars not flagged in Table 2 as having lower limit periods, and second using only RRab stars with $\Delta V > 0.9$. The results are listed in Table 4. As expected, for the most part the values calculated using all the RRab stars are slightly bluer than those which exclude the stars with lower limit periods. However, the offsets are not constant. We note that the recalculations for Fornax 1 and Fornax 5 each involved less than 5 stars (since several objects do not have $(V - I)_m$ measurements), so these two values are strongly subject to stochastic effects. Over the combined ensemble of all stars, the two recalculation values are 8×10^{-4} mag redder and 3×10^{-3} mag redder than the original calculation, respectively. We therefore conclude that the systematic effect is small (as predicted in Section 3.4), and we feel confident in using the four original values of $\langle (V - I)_m \rangle$ quoted above.

It is then a simple matter to show that for the four clusters $E(V - I) = 0.10, 0.07, 0.05$, and 0.04 . Errors in each of these values are ± 0.01 random and ± 0.03 systematic (from the value of $[(V - I)_m]_0$ determined by Mateo et al. (1995)). Adopting the reddening laws calculated in Mackey & Gilmore (2003b), we used these colour excesses to calculate A_V and $E(B - V)$ for each cluster. All of these quantities are listed in Table 4. The four $E(V - I)$ values we obtained match previous measurements well. For example, Buonanno et al. (1998b) determined $E(V - I) = 0.05, 0.09, 0.05$, and 0.08 (all ± 0.06) for the four clusters, using their red giant branches.

4.5 Horizontal Branch morphology

Quantitative measurements of the numbers and colours of RR Lyrae stars in the Fornax clusters allows a new determination of their horizontal branch morphologies and types. Fig. 5 shows a CMD of the HB region in each cluster. The RR Lyrae stars and candidate variables are plotted according to their identification – RRab stars are circles, RRc stars are triangles, and candidates are crosses. Stars with uncertain classification have hollow points (circles or triangles). For each cluster, the edges of the instability strip appear well defined. RRc stars fall toward the blue edge and RRab stars toward the red edge, although there appears to be some mixing of the two. This may be intrinsic, or it might be due to colour and classification uncertainties (although these effects should be small).

We note that Fornax 3 has four RR Lyrae type objects which are ~ 0.5 mag brighter than the main HB. The identity of these objects is not clear. It might be that they are interlopers from the field of the Fornax dwarf itself – cluster 3 has the highest level of background stars of the four clusters considered here (Demers, Irwin & Kunkel (1994)). Alternatively, they might be unusual cluster members, such as Population II cepheids or anomalous cepheids. Buonanno (1985) also identified one such candidate star in Fornax 3. We note that these four stars (F3V01, F3V07, F3V88, and F3V94) appear centrally concentrated, with three having radial distances $r \leq 16''$. This suggests that at least some of these stars are cluster members, and worthy of further investigation.

We can measure the intrinsic red and blue edges of the instability strip in each cluster from the colours of its RR Lyrae stars, and the colour excesses derived above. The four clusters seem particularly suitable for this type of measurement, with each possessing a very well populated horizontal branch (excepting cluster 1). Examining each edge, we see that in general there is some

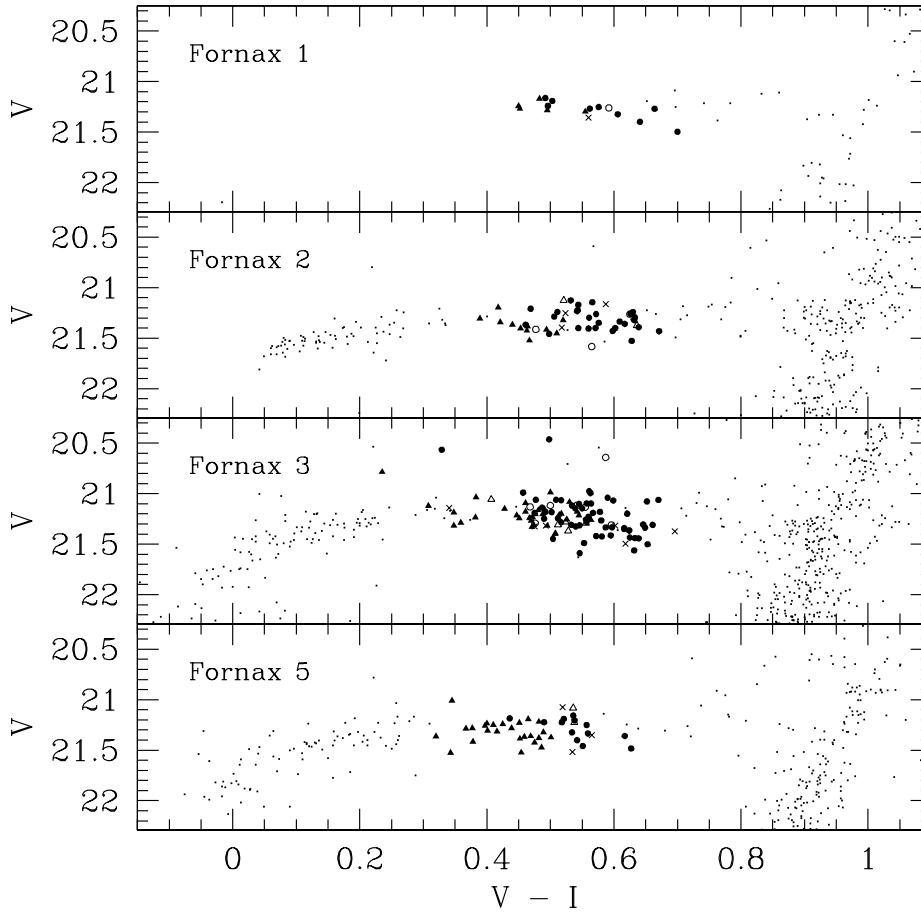


Figure 5. Colour-magnitude diagrams for each of the four clusters, showing their horizontal branch regions. The RR Lyrae stars are plotted. RRab stars are solid circles, and RRC stars solid triangles. Those stars with uncertain classification have hollow points. The candidate variable stars are plotted with crosses. Small dots represent non-variable objects.

small mixing of variable and non-variable stars. In addition, in some cases (e.g., the red edge for Fornax 2) one variable star lies quite distinct from the remainder. To account for these two effects, we choose an “edge” to be the mean colour of the two most extreme variable stars. Using this definition, we have calculated the colours $(V - I)_{RE}$ and $(V - I)_{BE}$ of the red and blue edges for each cluster[¶]. These quantities are listed in Table 2, along with their de-reddened counterparts. There is good agreement between the de-reddened measurements of the red edge. We obtain a mean $(V - I)_{RE} = 0.59 \pm 0.02$. The blue edge is more poorly defined. The HB for Fornax 1 does not extend to non-variable stars, so we can discount the measurement for this cluster. Similarly, while the Fornax 2 HB has a significant population of BHB stars, there is a gap at the blue edge of the RR Lyrae strip. Hence, $(V - I)_{BE}$ for this cluster is also ill-defined. For the well populated clusters Fornax 3 and 5, we obtain good agreement in the blue edge colour, with both having $(V - I)_{BE} = 0.28$. Applied to Fornax 2, this value has excellent consistency, with the reddest non-variable BHB

stars having intrinsic colours $V - I \sim 0.27$. We therefore adopt a mean $(V - I)_{BE} = 0.28 \pm 0.02$.

Finally, we can calculate the index $(B - R)/(B + V + R)$ of Lee, Demarque & Zinn (1994) (hereafter referred to as the HB type). In this quantity, B is the number of BHB stars in a cluster, R is the number of RHB stars, and V the number of HB variable stars – in our notation these are N_{BHB} , N_{RHB} , and N_{VHB} respectively. In general, $N_{VHB} \neq N_{RR}$, because we include N_{cand} in the count, and have the possibility of excluding some of the stars counted in N_{RR} – e.g., the four bright variables in Fornax 3. If we initially ignore the possibility of field star contamination, we count N_{RHB} as the number of stars with $20.8 < V < 21.7$ and $0.59 < (V - I)_0 < 0.77$. The red edge was chosen after careful consideration of the CMDs from the cluster centres, so as not to include any RGB stars. The value is in excellent agreement with that adopted for M54 by Layden & Sarajedini (2000). The BHB stars are easier to count, since this is an isolated area in each cluster’s CMD. We estimated the errors in N_{RHB} and N_{BHB} by counting the number of stars lying close to the edges of the defined regions. This gives some idea of the number of stars which might have been scattered in or out of these regions. We estimated the error in N_{VHB} by counting the number of non-variable stars lying in the RR Lyrae strip, and adding this to N_{cand} . This accounts

[¶] We did not include the four “bright” variable stars in the calculation for Fornax 3.

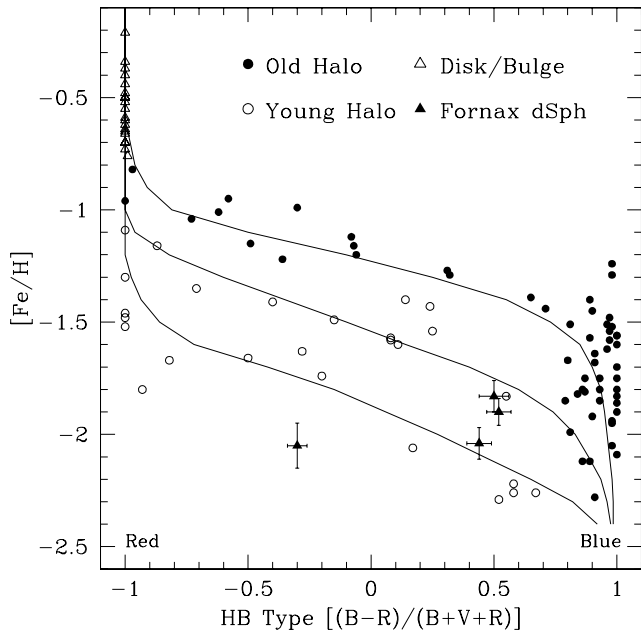


Figure 6. HB type versus metallicity diagram for the galactic globular clusters and the Fornax clusters from the present paper. The galactic clusters are split into three subsystems according to the criteria of Zinn (1993). The Fornax clusters are most similar to the galactic young halo population. The overplotted isochrones are from Rey et al. (2001) and constitute the latest versions of the Lee et al. (1994) synthetic HB models. The two lower isochrones are respectively 1.1 Gyr and 2.2 Gyr younger than the top isochrone.

for stars which we may have mis-identified as variable, or variable stars which were missed by our detection procedure. All star counts are listed in Table 2.

Using these quantities, we measured HB types of -0.30 ± 0.04 , 0.42 ± 0.05 , 0.40 ± 0.05 , and 0.52 ± 0.04 for the four clusters. The errors were derived using the quadrature formula in Smith et al. (1996). Our measurements are in reasonable agreement with the values derived by Buonanno et al. (1998b) using the same WFPC2 observations, but different numbers of variable stars (see Section 3.3). However, there is the possibility that our counts as described above have been contaminated by field stars, especially for clusters 2 and 3, which lie against significant backgrounds (see e.g., Demers et al. (1994)). In particular, these two clusters seem to have quite well populated red clumps on the RGB near the RHB, and it is therefore likely our measured HB types are too red. We have no nearby field observations, so to try and account for this we re-calculated the HB index for each cluster using only stars measured on the PC, where the cluster centres are imaged. In this case we derived HB types of -0.38 ± 0.06 , 0.50 ± 0.05 , 0.44 ± 0.05 , and 0.52 ± 0.05 , respectively. The calculation for cluster 1 involves small numbers of stars, and we prefer the original value. For the other three clusters, it is clear that Fornax 5 has not suffered any contamination (as expected – this cluster lies well separated from the dwarf galaxy), but Fornax 2 and 3 possess some small field star contamination. For these two clusters we prefer the HB types as calculated from the PC, rather than the original values.

Additionally, we note that the CMD for cluster 1 presented by Buonanno et al. (1996) apparently shows several HB stars bluer than $V - I \sim 0.3$, whereas these stars are not present in our data.

Hence our derived HB type for this cluster may be too red. It is possible that the WFPC2 observations did not include the region of Fornax 1 containing the BHB stars; however we find this explanation unlikely since the images cover ~ 75 per cent of the cluster, including its core. Even so, adding several BHB stars to the calculation does not produce a large effect. Four stars would move the HB type to ~ -0.1 , still in reasonable agreement with our preferred value.

These measurements confirm the existence of a “second parameter” effect among the Fornax globular clusters, as highlighted previously by several authors (Smith et al. 1996; Buonanno et al. 1998b). For example, clusters 1 and 3 have very similar metallicities (see Table 2), but extremely disparate HB morphologies. In Fig. 6 we plot a HB type versus metallicity diagram to highlight this result. Lee et al. (1994) have suggested that age differences can mostly account for second parameter variations in HB type, in that younger clusters possess redder horizontal branches at given $[\text{Fe}/\text{H}]$. Zinn (1993) split the galactic globular clusters by metallicity and HB type into three distinct groups. The most metal rich clusters are associated with the bulge and thick-disk of the galaxy, and the most metal poor with the halo. The halo clusters are subdivided into “young” and “old” groups on the basis of their HB type. From Fig. 6 it is clear that the Fornax clusters are most similar to the galactic young halo clusters. This is compatible with the assertion of Zinn (1993) that the young halo clusters have likely been accreted by the galaxy through merger events with satellite dwarf galaxies.

Buonanno et al. (1998b) have measured the ages of Fornax clusters 1, 2, 3, and 5 to be identical to within ± 1 Gyr, and equally coeval with the metal-poor galactic globular clusters M68 and M92. The isochrones overplotted on Fig. 6 show that based on HB type, the Fornax clusters should be more than 1.1 Gyr younger than the galactic old halo clusters, and moreover should have an internal age spread greater than ~ 1.1 Gyr (in that Fornax 1 should be younger). If the Buonanno et al. (1998b) ages are correct, then it is possible that age is not the sole second parameter operating in the Fornax clusters. Bearing in mind the extreme difference highlighted in Section 4.1 between the specific frequencies of RR Lyrae stars in the Fornax and galactic globular clusters, and the way that the HB index is defined, it seems likely that the relative number of RR Lyrae stars in a cluster has a significant bearing on the measured HB type. It is certainly interesting to note that the four galactic globular clusters with $S_{RR} > 60$ are all members of the galactic young halo population.

4.6 Distance and structure of the Fornax dwarf

Using the mean V magnitudes we measured for the RR Lyrae stars, it is also possible to determine a distance modulus to each cluster. To do this, we need to know the absolute magnitude $M_V(RR)$ of the RR Lyrae stars. This quantity is a function of metallicity, so that more metal poor stars are intrinsically brighter. We adopt the relation from the review of Chaboyer (1999):

$$M_V(RR) = 0.23([\text{Fe}/\text{H}] + 1.6) + 0.56 \quad (5)$$

which includes *Hipparcos* results. This is the same relation used by Layden & Sarajedini (Layden & Sarajedini 2000) to determine the distance to M54 and the Sagittarius dwarf galaxy. We note that the relation has an uncertainty of ± 0.12 mag in the zero-point term, reflecting the discrepancies which exist between the different techniques to determine $M_V(RR)$.

Table 4. Globular cluster and RR Lyrae population characteristics.

		Fornax 1	Fornax 2	Fornax 3	Fornax 5
N_{RR}		15	43	99	40
N_{cand}		1	3	6	3
M_V		-5.33	-7.05	-7.80	-7.05
S_{RR}	(Lower limits)	118.2	70.5	90.2	68.4
N_{ab}	(All RRab)	10	30	61	13
	(RRab with good P)	5	15	32	8
	(RRab with $\Delta V > 0.9$)	4	10	14	5
N_c		5	13	38	27
N_c/N_{RR}		0.33	0.30	0.38	0.68
$\langle P_{ab} \rangle$	(All RRab)	0.546	0.494	0.532	0.532
	(RRab with good P)	0.611	0.574	0.613	0.577
P_{tr}	(RRab with $\Delta V > 0.9$)	0.544	0.540	0.582	0.548
$\langle P_c \rangle$	(All RRc)	0.431	0.373	0.404	0.374
$\langle (V - I)_m \rangle$	(All RRab)	0.68 ± 0.01	0.65 ± 0.01	0.63 ± 0.01	0.62 ± 0.01
	(RRab with good P)	0.70 ± 0.01	0.66 ± 0.01	0.63 ± 0.01	0.60 ± 0.01
	(RRab with $\Delta V > 0.9$)	0.69 ± 0.01	0.66 ± 0.01	0.63 ± 0.01	0.60 ± 0.01
$E(V - I)$		0.10 ± 0.01	0.07 ± 0.01	0.05 ± 0.01	0.04 ± 0.01
$E(B - V)$		0.07 ± 0.01	0.05 ± 0.01	0.04 ± 0.01	0.03 ± 0.01
A_V		0.23 ± 0.02	0.16 ± 0.02	0.12 ± 0.02	0.10 ± 0.02
$(V - I)_{RE}$	Measured	0.68 ± 0.02	0.66 ± 0.02	0.66 ± 0.02	0.62 ± 0.02
	De-reddened	0.58 ± 0.03	0.59 ± 0.03	0.61 ± 0.03	0.58 ± 0.03
$(V - I)_{BE}$	Measured	0.45 ± 0.01	0.39 ± 0.02	0.33 ± 0.02	0.32 ± 0.01
	De-reddened	0.35 ± 0.02	0.32 ± 0.03	0.28 ± 0.03	0.28 ± 0.02
N_{BHB}	($\equiv B$) (All chips)	0 ± 0	68 ± 4	114 ± 15	83 ± 6
N_{RHB}	($\equiv R$) (All chips)	7 ± 1	14 ± 3	20 ± 4	12 ± 3
N_{VHB}	($\equiv V$) (All chips)	16 ± 2	46 ± 9	101 ± 15	43 ± 5
HB index	$\frac{(B-R)}{(B+V+R)}$ (All chips)	-0.30 ± 0.04	0.42 ± 0.05	0.40 ± 0.05	0.52 ± 0.04
	(PC only)	-0.38 ± 0.06	0.50 ± 0.06	0.44 ± 0.05	0.52 ± 0.05
[Fe/H]		-2.05 ± 0.10	-1.83 ± 0.07	-2.04 ± 0.07	-1.90 ± 0.06
$M_V(RR)$		0.46 ± 0.02	0.51 ± 0.02	0.46 ± 0.02	0.49 ± 0.02
$\langle V(RR) \rangle$	(All RR)	21.27 ± 0.01	21.34 ± 0.01	21.24 ± 0.01	21.33 ± 0.01
	(All RRab)	21.29 ± 0.01	21.32 ± 0.01	21.25 ± 0.01	21.35 ± 0.01
	(RRab with good P)	21.29 ± 0.01	21.31 ± 0.01	21.21 ± 0.01	21.32 ± 0.01
	(RRab with $\Delta V > 0.9$)	21.29 ± 0.01	21.29 ± 0.01	21.20 ± 0.01	21.30 ± 0.01
	(All RRc)	21.26 ± 0.01	21.36 ± 0.01	21.21 ± 0.01	21.30 ± 0.01
$(m - M)_0$		20.58 ± 0.05	20.67 ± 0.05	20.66 ± 0.05	20.74 ± 0.05
Distance	(kpc)	130.6 ± 3.0	136.1 ± 3.1	135.5 ± 3.1	140.6 ± 3.2

To obtain metallicities for each cluster, we used the recent measurements and literature collation of Strader et al. (2003). From their Table 5, we calculated the mean measured metallicity for each cluster. This combines the results of several different measurement techniques, ranging from integrated spectroscopy to the slope of the RGB. For the four clusters, we obtain $[\text{Fe}/\text{H}] = -2.05 \pm 0.10$, -1.83 ± 0.07 , -2.04 ± 0.07 , and -1.90 ± 0.06 . This results in RR Lyrae absolute magnitudes of $M_V(RR) = 0.46 \pm 0.02$, 0.51 ± 0.02 , 0.46 ± 0.02 , and 0.49 ± 0.02 , respectively.

The next step is to obtain a mean V RR Lyrae magnitude, $\langle V(RR) \rangle$ for each cluster. We determined these from the $\langle V \rangle$ measurements in Table 2. Stars with $\langle V \rangle$ deviant by more than 2σ were not included in the final average. The mean V magnitudes so ob-

tained are listed in Table 4. Using the extinction values calculated above, together with the RR Lyrae absolute magnitudes, we then determined a distance modulus for each cluster. These results are also listed in Table 4. The mean distance modulus is 20.66 ± 0.03 mag, which is in good agreement with previously determined values. In particular, Buonanno et al. (1999) obtain an estimate of 20.68 ± 0.20 to the centre of the Fornax dwarf (i.e., cluster 4) after a thorough discussion of several techniques and literature measurements. We note that the uncertainties quoted for our results are due to random errors only, and that there are also systematic errors totalling approximately ± 0.15 mag.

In addition we briefly investigated the likelihood that our $\langle V(RR) \rangle$ values are systematically too faint, based on the discus-

sion in Section 3.4. We recalculated $\langle V(RR) \rangle$ using only RRab stars, then only RRab stars with good periods, and then only RRab stars with $\Delta V > 0.9$. These values are also listed in Table 4. On average, the $\langle V(RR) \rangle$ calculated using all the RRab stars are ~ 0.03 mag fainter than those calculated using the RRab stars with good periods, and ~ 0.04 mag fainter than those calculated using the RRab stars with $\Delta V > 0.9$. This demonstrates exactly what we argued in Section 3.4 – that we expect a systematic error in $\langle V(RR) \rangle$ due to our short observation baselines. If we include the RRc stars in our calculations, the offsets are moderated somewhat. The two worst affected clusters are Fornax 3 and 5, which may have distance moduli 0.03 mag closer than those we have quoted.

Our distance moduli correspond to distances of 130.6 ± 3.0 kpc, 136.1 ± 3.1 kpc, 135.5 ± 3.1 kpc, and 140.6 ± 3.2 kpc for the four clusters. Again, the quoted uncertainties reflect random errors only. These measurements are consistent with, but do not require, a significant line of sight depth to the Fornax system, with a value of ~ 10 kpc. The outlying clusters are Fornax 1 and 5, which are also the clusters with the greatest angular separation from the centre of the Fornax dwarf (see Mackey & Gilmore (2003b)). We note that if Fornax 5 is indeed 0.03 mag closer than we have listed above, the line of sight depth shrinks slightly to ~ 8 kpc. Demers et al. (1994) obtained a tidal radius for Fornax of $r_t = 77 \pm 10$ arcmin along the minor axis, and an ellipticity of 0.27 at this radius. Hence the tidal radius along the major axis must be 105 ± 14 arcmin. These radii correspond to linear distances of 7.0 ± 0.9 kpc and 9.6 ± 1.3 kpc at our mean distance modulus of 20.66. These are of a similar magnitude to the ~ 4.5 kpc radius obtained from our line of sight depth, suggesting that Fornax is close to spherical. This lack of extended line of sight depth argues against models of dSph galaxies which invoke very large line of sight depth and/or tides to explain the observed high stellar velocity dispersions. Other recent studies have reached a similar conclusion (e.g., Klessen, Grebel & Harbeck (2003), who studied the thickness of the Draco dSph HB). It seems most likely that dSph galaxies with high stellar velocity dispersions constitute dark matter dominated systems.

5 SUMMARY AND CONCLUSIONS

We have identified and measured 197 RR Lyrae stars in four of the globular clusters in the Fornax dwarf galaxy, using archival WFPC2 observations. We also located 13 variable HB objects, which are likely RR Lyrae stars. A typical star in our sample has 14 paired F555W and F814W observations spread over ~ 0.36 days. Such a short baseline has compromised our ability to measure accurate periods for ~ 50 per cent of the RRab type stars we identified – for these objects we instead calculated lower limits for the oscillation periods and amplitudes. Nonetheless, we have successfully determined periods for all the RRc and 50 per cent of the RRab stars in the ensemble. We also present measurements of mean magnitudes and colours for all the objects in our sample, and discuss the introduction of systematic errors into these calculations due to our short observational baseline. This is the first time that RR Lyrae stars have been identified in these clusters, and quantitative measurements of their variability presented. Naturally, additional observations at more than one epoch will be extremely useful in refining our classifications and measurements, and in particular in allowing good periods to be determined for all stars.

Even given the difficulties associated with measuring periods for some of the sample, we have been able to obtain a large amount of useful information about the Fornax globular clusters from the

RR Lyrae stars. The specific frequencies of the four clusters are exceptionally large in comparison to those for the galactic globular clusters. All of the four Fornax clusters have $S_{RR} > 80$, while only four of the ~ 150 galactic clusters have such large values. It is likely that Fornax 1 has the largest specific frequency ever measured in a globular cluster. The Fornax clusters are also unusual in that their RR Lyrae populations possess mean properties which lie intermediate between the two Oosterhoff groups defined by the galactic globular clusters. In this respect the RR Lyrae stars in the Fornax clusters are similar to those in the old LMC clusters, but most resemble the field populations of several dwarf galaxies. Fornax cluster 5 stands out in having an extremely high fraction of RRc stars ($N_c/N_{RR} \sim 0.6$), and possessing four strong RRe (second overtone pulsator) candidates.

Using the mean RR Lyrae colours at minimum light, we have measured colour excesses and line of sight extinction values towards the four clusters. With a significant catalogue of HB variable stars, we have also been able to provide new estimates of the HB morphology in these clusters. We have confirmed the presence of the second parameter effect, in particular between clusters 1 and 3, which have identical metallicities and ages, but extremely different HB morphology. The HB morphologies of the Fornax clusters are in general redder than many galactic clusters of similar metallicity – in this respect they most resemble the “young” galactic halo population. We also find good agreement between measurements of the intrinsic red and blue edges to the instability strip at the HB. We determine $(V-I)_{RE} = 0.59 \pm 0.02$ and $(V-I)_{BE} = 0.28 \pm 0.02$.

Finally, we have used the mean RR Lyrae brightnesses to determine the distance to the Fornax dwarf galaxy. We measure a mean distance modulus of $(m-M)_0 = 20.66 \pm 0.03$ mag, which is in excellent agreement with previous measurements. Our calculations are consistent with a line of sight depth of $\sim 8 - 10$ kpc for the Fornax dwarf galaxy. This value is in good accordance with the dimensions of this galaxy as measured in the plane of the sky, and argues against the tidal-remnant models of dSph galaxies which are invoked to explain their observed internal stellar dynamics.

ACKNOWLEDGMENTS

ADM would like to acknowledge the support of a Trinity College ERS grant and a British government ORS award. We would also like to thank Andrew Layden for making his template-fitting programs publicly available. This paper is based on observations made with the NASA/ESA *Hubble Space Telescope*, obtained from the data archive at the Space Telescope Institute. STScI is operated by the association of Universities for Research in Astronomy, Inc. under the NASA contract NAS 5-26555.

REFERENCES

- Bersier D., Wood P. R., 2002, *AJ*, 123, 840
- Buonanno R., Corsi C. E., Fusi Pecci F., Hardy E., Zinn R., 1985, *A&A*, 152, 65
- Buonanno R., Corsi C. E., Ferraro F. R., Fusi Pecci F., Bellazzini M., 1996, in Morrison H. L., Sarajedini A., eds., *ASP Conf. Ser. Vol. 92, Formation of the Galactic Halo – Inside and Out*. Astron. Soc. Pac., San Francisco, p. 520
- Buonanno R., Corsi C. E., Zinn R., Fusi Pecci F., Hardy E., Suntzeff N. B., 1998, *ApJ*, 501, L33
- Buonanno R., Corsi C. E., Castellani M., Marconi G., Fusi Pecci F., Zinn R., 1999, *AJ*, 118, 1671

- Chaboyer B., 1999, in Heck A., Caputo F., eds., *Post-Hipparcos Cosmic Candles*. Kluwer, Dordrecht, p. 111
- Clement C. M., Rowe J., 2000, *AJ*, 120, 2579
- Dall’Ora M., et al., 2003, *astro-ph/0302418*
- Demers S., Kunkel W. E., Grondin L., 1990, *PASP*, 102, 632
- Demers S., Irwin M. J., Kunkel W. E., 1994, *AJ*, 108, 1648
- Dolphin A. E., 2000a, *PASP*, 112, 1383
- Dolphin A. E., 2000b, *PASP*, 112, 1397
- Harris W. E., 1996, *AJ*, 112, 1487
- Hodge P. W., 1961, *AJ*, 66, 83
- Holtzman J., et al., 1995, *PASP*, 107, 1065
- Klessen R. S., Grebel E. K., Harbeck D., 2003, *ApJ*, in press
- Kleyna J. T., Wilkinson M. I., Gilmore G., Evans N. W., 2003, *ApJ*, 588, L21
- Layden A. C., 1998, *AJ*, 115, 193
- Layden A. C., Sarajedini A., 2000, *AJ*, 119, 1760
- Layden A. C., Ritter L. A., Welch D. L., Webb T. M. A., 1999, *AJ*, 117, 1313
- Lee Y. -W., Demarque P., Zinn R., 1994, *ApJ*, 423, 248
- Mackey A. D., Gilmore G. F., 2003a, *MNRAS*, 338, 85
- Mackey A. D., Gilmore G. F., 2003b, *MNRAS*, 340, 175
- Maio M., et al., *astro-ph/0303666*
- Mateo M., Udalski A., Szymanski M., Kaluzny J., Kubiak M., Krzeminski W., 1995, *AJ*, 109, 588
- Pritzl B. J., Armandroff T. E., Jacoby G. H., Da Costa G. S., 2002, *AJ*, 124, 1464
- Rey S. -C., Yoon S. -J., Lee Y. -W., Chaboyer B., Sarajedini A., 2001, *AJ*, 122, 3219
- Sandage A., 1990, *ApJ*, 350, 603
- Sandage A., 1993, *AJ*, 106, 703
- Smith E. O., Neill J. D., Mighell K. J., Rich R. M., 1996, *AJ*, 111, 1596
- Smith E. O., Rich R. M., Neill J. D., 1997, *AJ*, 114, 1471
- Smith H. A., 1995, *RR Lyrae Stars*. Cambridge Univ. Press, Cambridge
- Strader J., Brodie J. P., Forbes D. A., Beasley M. A., Huchra J. P., 2003, *AJ*, 125, 1291
- Webbink R. F., 1985, in Goodman J., Hut P., eds., *Proc. IAU Symp.* 113, *Dynamics of Star Clusters*. Kluwer, Dordrecht, p. 541
- Welch D. L., Stetson P. B., 1993, *AJ*, 105, 1813
- Zinn R., 1993, in Smith G. H., Brodie J. P., eds., *ASP Conf. Ser. Vol. 48, The Globular Cluster-Galaxy Connection*. Astron. Soc. Pac., San Francisco, p. 303
- Zinn R., West M. J., 1984, *ApJS*, 55, 45

This paper has been produced using the Royal Astronomical Society/Blackwell Science \LaTeX style file.